Chapter 5

Resilience-Oriented Scheduling of DC Microgrid Considering Participation in the Automatic Frequency Regulation Reserves market

5.1 Introduction

The DCμG architecture offers significant advantages over its AC counterpart, such as eliminating frequency synchronisation and reactive power management challenges, making it ideal for applications like rural electrification, community buildings, and data centers [7]. A robust EMS for DCμGs aims to ensure economic efficiency, operational stability, and resilience, addressing challenges such as intermittent RES generation, limited controllable capacity, and emergency scenarios.

Beyond economic scheduling of DER, participation in reserve markets like aFRR enhances the financial viability of DCμGs. Interfaced with the upstream AC grid via a GIC, DCμGs can utilise their flexible resources to meet internal demand while offering surplus active power in reserve markets [103]. This integration provides additional revenue streams, making operations financially attractive for the DCμGO.

Emergencies and natural disasters, such as windstorms and hurricanes, further complicate DCμG operations. In such scenarios, grid and renewable unit disconnection are necessary to prevent widespread damage, while uninterrupted power supply must be ensured for critical loads like hospitals, military facilities, and data centres. The capability of a power system to maintain stable operation during high-impact, low-probability events is defined as resilience [11, 12, 13]. A purely economic EMS often fails to meet critical load demands in emergencies [14], underscoring the need to incorporate resilience into the EMS design.

The challenges of RES generation volatility and resilience can be addressed by integrating electricity and H_2 systems. The global push for carbon-free fuels has positioned H_2, produced via water electrolysis (P2H), as a clean and efficient energy carrier [71]. HSS offers high energy density, long-term storage potential, and abundant backup energy during emergencies, enhancing resilience and enabling arbitrage benefits [72, 73]. Combining HSS with BESS in a hybrid energy storage system (HESS) provides both long-term autonomy and rapid transient response, reducing RES curtailment and offering grid flexibility [74].

Moreover, P2H units act as controllable loads, enabling demand-side flexibility. Green H_2 produced by RES can be converted back to electricity through H2P units during low RES output or high energy prices, supporting economic competitiveness and resilient operation. Thus, integrating electricity-H_2 systems within the EMS framework can decarbonise the energy system, firm RES generation, and enhance the operational robustness of DCμGs under both normal and emergency conditions.

Therefore, the aim of this chapter is to study the mutual interdependence between electricity and H_2 sector within a DCμG architecture, leverage the flexibility of the HESS comprising high energy density HSS and high power density BESS for developing a resilience-oriented economic EMS for an electricity-H_2 DCμG with aFRR participation capability to address the challenges of DCμG operation mentioned above.

A detailed literature survey has been presented in **section 1.3**. A comparison of contributions made by relevant papers with the work done in this chapter is given in table 5.1. The following gap areas are found in the existing literature:

- **Gap#1)**: To the best of the author's knowledge, investigation of interaction and interdependence between electricity and H_2 systems with proper co-optimal schedul-

Table 5.1: Summary of literature review

Ref.	Uncertainty modelling					BESS	P2H/H2P unit	Resilient Operation	Reserve Market Constraints	DCμG Network Constraints	Objective
	A	B	C	D	E						
[82]	✗	✗	✗	✗	✗	✓	✓	✗	✗	✓	Cost minimisation
[15]	✗	✗	✗	✗	✗	✓	✗	✗	✗	✗	Improving voltage stability
[16]	✗	✗	✗	✗	✗	✓	✗	✗	✗	✗	Investment cost minimisation
[83]	✗	✗	✗	✗	✗	✓	✓	✗	✗	✗	Reliability improvement
[19]	✗	✗	✗	✗	✗	✗	✗	✗	✗	✓	Power loss minimisation and voltage improvement
[84]	✗	✗	✗	✗	✗	✓	✓	✗	✗	✗	Cost minimisation
[104]	✗	✗	✗	✗	✗	✓	✗	✗	✗	✓	Cost minimisation
[22]	✗	✗	✗	✗	✗	✓	✗	✗	✗	✗	Cost minimisation
[25]	✗	✗	✗	✗	✗	✓	✗	✗	✗	✗	Voltage profile improvement
[87]	✗	✗	✗	✗	✗	✓	✓	✗	✗	✗	Stability improvement
[33]	✗	✗	✗	✗	✗	✓	✗	✗	✗	✗	Voltage profile improvement
[50]	✓	✗	✗	✗	✗	✓	✗	✗	✗	✗	Voltage profile improvement
[52]	✓	✗	✗	✗	✗	✓	✗	✗	✗	✓	Cost minimisation
[60]	✗	✗	✓	✗	✗	✓	✓	✗	✗	✓	Voltage profile improvement
[61]	✗	✓	✓	✗	✗	✗	✗	✗	✗	✓	Cost and emission reduction
[64]	✓	✗	✓	✗	✗	✓	✗	✗	✗	✓	Cost minimisation and voltage improvement
[70]	✗	✗	✓	✗	✓	✗	✗	✗	✗	✓	Cost minimisation and voltage improvement
[75]	✗	✗	✗	✗	✗	✓	✓	✗	✗	✗	Cost minimisation
[79]	✗	✗	✗	✗	✗	✓	✓	✗	✗	✗	Cost minimisation
[80]	✗	✗	✗	✗	✗	✓	✓	✗	✗	✗	Cost minimisation
[81]	✗	✗	✗	✗	✗	✓	✓	✗	✗	✗	Cost minimisation
[77]	✗	✗	✗	✗	✗	✓	✓	✗	✗	✗	Cost minimisation
[78]	✗	✗	✗	✗	✗	✓	✓	✗	✗	✗	Cost minimisation
[85]	✗	✗	✗	✗	✗	✓	✓	✗	✗	✗	Reliability improvement
[12]	✗	✗	✗	✗	✗	✓	✓	✓	✗	✗	Cost minimisation and resilient operation
[14]	✗	✗	✗	✗	✗	✗	✗	✓	✗	✗	Critical load restoration
[74]	✗	✗	✗	✗	✗	✓	✓	✓	✗	✗	Storage optimisation resilient operation
[109]	✗	✗	✗	✗	✗	✓	✗	✓	✗	✗	Cost minimisation resilient operation
[108]	✗	✗	✗	✗	✗	✓	✓	✗*	✗	✗	Cost minimisation resilient operation
[110]	✗	✗	✗	✗	✗	✓	✗	✓	✗	✗	Economic and resilient operation
[111]	✗	✗	✗	✗	✗	✓	✗	✓	✗	✗	Cyber-attack resilient operation
[112]	✗	✗	✗	✗	✗	✗	✗	✓	✗	✗	Information-islanding resilient operation
[113]	✗	✗	✗	✗	✗	✗	✗	✓	✗	✗	DoSA resilient operation
[115]	✗	✗	✗	✗	✗	✗	✗	✓	✗	✗	Cyber-attack resilient operation
[116]	✗	✗	✗	✗	✗	✗	✗	✓	✗	✗	DoSA resilient operation
[117]	✗	✗	✗	✗	✗	✗	✗	✓	✗	✗	Cyber-attack resilient operation
[118]	✗	✗	✗	✗	✗	✗	✗	✓	✗	✗	DoSA and FDIA resilient operation
[119]	✗	✗	✗	✗	✗	✗	✗	✓	✗	✗	MITM resilient operation
[120]	✗	✗	✗	✗	✗	✓	✗	✓	✗	✗	Resilience for DC bus voltage stability
[121]	✗	✗	✗	✗	✗	✓	✗	✓	✗	✗	DoSA resilient operation
[122]	✗	✗	✗	✗	✗	✓	✗	✓	✗	✗	unknown cyber-attack resilient operation
[123]	✗	✗	✗	✗	✗	✓	✗	✓	✗	✗	DoSA resilient operation
[124]	✗	✗	✗	✗	✗	✗	✗	✓	✗	✗	FDIA resilient operation
[92]	✓	✗	✓	✗	✗	✓	✗	✗	✓	✗	Profit maximisation
[93]	✓	✓	✗	✗	✗	✗	✗	✗	✓	✗	Profit maximisation
[94]	✗	✓	✗	✓	✗	✗	✓	✗	✓	✗	Profit maximisation
[95]	✗	✗	✗	✗	✗	✓	✗	✗	✓	✗	Profit maximisation
[96]	✗	✓	✗	✗	✗	✓	✗	✗	✓	✗	Profit maximisation
[97]	✗	✗	✗	✗	✗	✗	✗	✗	✓	✗	Profit maximisation
[98]	✗	✗	✗	✗	✗	✓	✗	✗	✓	✗	Profit maximisation
[99]	✓	✓	✗	✗	✗	✓	✗	✗	✓	✗	Profit maximisation
[100]	✗	✗	✗	✗	✗	✓	✗	✗	✓	✗	Frequency and stability improvement
[101]	✗	✗	✗	✗	✗	✗	✓	✗	✓	✗	Profit maximisation
[102]	✗	✗	✗	✗	✗	✓	✗	✗	✓	✗	Profit and stability maximisation
Proposed	✓	✓	✓	✓	✓	✓	✓	✓	✓	✓	**Economic and resilient operation**

A: Wind; B:wholesale market electricity price; C: Load Demand; D: H_2 Demand; E: Correlation; *: Only islanded condition

ing for participation in the aFRR market has not been reported for a DCμG system considering DCμG network model and network operating constraints. The electricity-H_2 sectoral coupling and participation in the aFRR market were not considered in most of the reported studies on DCμG EMS [15, 16, 19, 22, 25, 33, 50, 52, 60, 61, 64, 70, 82, 83, 84, 87, 104, 198]. On the other hand, studies available on the co-optimisation of electricity and H_2 systems mostly pertain to either AC networks or integrated energy systems where either AC networks have been considered, or network models of the power system have been neglected altogether [12, 77, 78, 106, 107, 108]. Also, as far as the authors know, investigations of DCμG EMS considering DCμG participation in the frequency reserve/ aFRR market with DCμG network model, network, and unit level operating constraints have not been reported so far [92, 93, 94, 95, 96, 97, 98, 99, 100, 101, 102]. Since the DCμG network model along with DCμG network operating constraints were not considered in the above studies [12, 77, 78, 92, 93, 94, 95, 96, 97, 98, 99, 100, 101, 102, 106, 107, 108], the optimal schedule generated by the EMS may cause a violation of DCμG operational constraints like line current and bus voltage limits. Therefore, the reported studies cannot be extended directly to a DCμG network.

- **Gap#2**): Most studies on resilient operation of DCμGs focused on cyber-security aspects and not on energy scheduling of DCμGs for uninterrupted electricity supply to critical loads and minimisation of curtailment of non-critical loads after islanding due to an extreme event [110, 111, 112, 113, 115, 116, 117, 118, 119, 120, 121, 122, 123, 124]. On the other hand, studies dealing with resilience-oriented EMS pertain to either AC networks or integrated energy hubs, in which either AC power system models or lumped power system models (network equations and network operating security constraints ignored) have been considered [12, 14, 74, 109]. Therefore, the above-mentioned resilience-oriented scheduling schemes cannot be extended directly to DCμGs because of the risk of violation of DCμG network operating security constraints (line current and bus voltage limits).

- **Gap#3**): To the best of the author's knowledge, no reported study has so far investigated the impact of the length of the proactive preparation period in a resilience-oriented economic scheduling scheme on the operating economy (normal and proac-

tive preparation) and load (critical and non-critical) curtailment in the emergency period [12, 14, 74, 109].

Hence, there is a lack of comprehensive study on DCμG EMS encompassing interaction and interdependence between H_2 and electricity sectoral coupling together with resilience aspect and participation in the aFRR market considering a DCμG network model, unit and network level constraints. To the best of the authors' knowledge, no published work on DCμG has considered resilience, aFRR participation and economical operation with network and system level models and constraints simultaneously to date. The motivation of the current study is to bridge the above gap. In this chapter, we propose a methodology for the practical coordination of resilience-oriented economic operation of an electricity-H_2 DCμG with aFRR market participation and DCμG network operational constraints. Specific contributions are as follows:

- **Contribution#1**): A resilience oriented economic model predictive control based EMS (R-MPCE) is proposed for a DCμG involving co-optimisation of H_2 and electrical systems. The objectives of the R-MPCE are to ensure economical operation along with aFRR market participation during normal operating periods, economically impose a proactive preparation period before extreme events, and serve critical loads with minimum curtailment of non-critical loads after islanding during the emergency period. The R-MPCE is designed considering the network model of the DCμG together with the equipment and network level constraints to ensure that the optimal schedule does not violate the system's operational constraints. Therefore, gap area #1 and gap area #2 are addressed.

- **Contribution#2)**: Additional network and equipment-level constraints for participation in the aFRR market are explicitly designed and incorporated in the EMS so that no operational constraints are violated when the DCμG participates in the aFRR market during grid-connected operation. Therefore, gap area #1 is addressed.

- **Contribution#3)**: The impact of the length of the proactive preparation period in the R-MPCE on the cost of DCμG operation and load curtailment is investigated to bridge gap area #3. The subject analysis will act as a guide for the judicious selection of the proactive preparation period.

- **Contribution#4)**: The uncertainties of RES generation and load demand, along with the correlation between input RVs, are incorporated using probabilistic Copula models to mitigate the risk of dispatching EMS in an uncertain environment.

The chapter is structured as follows: **section 5.2** covers the operational framework and uncertainty modelling, laying the groundwork for the study. In **section 5.3** and **section 5.4**, the problem formulation is thoroughly discussed. We present the simulation studies and results with a detailed evaluation of the proposed approach in **section 5.5**. Finally, **section 5.6** concludes the chapter.

5.2 Operational Framework and Uncertainty Modelling

5.2.1 System configuration and operating framework

In the proposed work, the DCμG consists of various DER. The DER include WPG, a BESS, a HSS, a FC, an AE, and a MT. The DCμG is connected to the upstream AC grid using a GIC, which acts as the slack node. The DCμGO buys/sells electricity from/to the upstream AC grid at the wholesale market electricity price. Three load types are considered: "flexible", "moderate", and "critical" [12]. Three operating periods are defined, namely, the normal operating period, the proactive preparation period, and the emergency operating period. During the normal period, all the flexible and nonflexible units are coordinated to maximise profit while feeding all three load types (flexible, moderate, and critical). Also, during this period, the DCμG participates in the electricity and gas (H_2) energy markets and the aFRR market. Before extreme events, i.e., the emergency period, a proactive preparation strategy is adopted using the receding horizon concept in the EMPC formulation. A proactive preparation period allows the DCμG to prepare itself for the upcoming extreme events so that critical loads can be supplied during the emergency period for a horizon equal to a normal schedule (i.e., 24 hours in this work), thus meeting the criticality criterion [207]. During the emergency period, WPG and grid are disconnected from the DCμG to prevent the propagation of adverse impact and avoid potential device damage. Also, AE is disconnected so that proper reserves can be utilised to feed the loads. During the emergency, the sole objective is to feed the critical loads

Table 5.2: Probabilistic Uncertainty Modelling of input RVs

Parameter	Distribution	pdf	Correlated/Uncorrelated
H_2 demand ($m_t^{H_2,d}$)	Normal	$f_{H_2}(m_t^{H_2,d}) = \frac{1}{\sigma_t^{H_2,d}\sqrt{2\pi}} exp\left[-\frac{\left(m_t^{H_2,d}-\mu_t^{H_2,d}\right)^2}{2(\sigma_t^{H_2,d})^2}\right]$	Uncorrelated
WPG power (PW_t^b)	Weibull	$f_W(PW_t^b) = \frac{x_t^b}{c_t^b}\left(\frac{PW_t^b}{c_t^b}\right)^{(x_t^b-1)} \exp\left[-\left(\frac{PW_t^b}{c_t^b}\right)^{x_t^b}\right]$	Correlated
Load (PL_t^b)	Normal	$f_{load}(PL_t^b) = \frac{1}{\sigma_{l,t}^b\sqrt{2\pi}} exp\left[-\frac{\left(PL_t^b-\mu_{l,t}^b\right)^2}{2(\sigma_{l,t}^b)^2}\right]$	Correlated
Wholesale electricity price (π_t^g)	Normal	$f_{price}(\pi_t^g) = \frac{1}{\sigma_{g,t}\sqrt{2\pi}} exp\left[-\frac{\left(\pi_t^g-\mu_{g,t}\right)^2}{2(\sigma_{g,t})^2}\right]$	Correlated

while minimizing the load shedding of flexible and moderate electricity consumers and H_2 consumers.

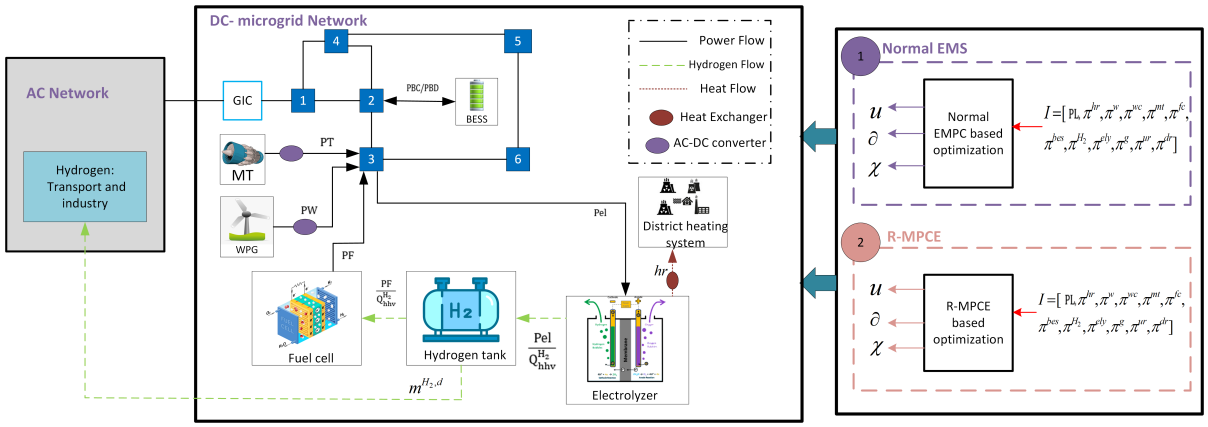

Figure 5.1: Configuration of DCμG

5.2.2 Uncertainty Modelling

Uncertain RVs are power generated by the WPG, electrical and H_2 demand, and wholesale electricity price. The uncertain RVs are modelled in the probabilistic framework using pdf. The H_2 demand is assumed to be uncorrelated with the other two input RVs and modelled using "Normal distribution". The RES generation, the electricity demand, and the power price in the day-ahead market are considered to be correlated. "Copula" theory is used to model the correlation between RVs. Rank correlation measures the correlation between two input RVs. Let X_1 and X_2 be the two input RVs with cdfs, $F_{X1}(x_1)$ and $F_{X2}(x_2)$. Then rank correlation ($\rho_r(X_1, X_2)$) is given as:

$$\rho_r(X_1, X_2) = \rho_m(F_{X1}(x_1), F_{X2}(x_2)) \tag{5.1}$$

Where, $\rho_m(F_{X1}(x_1), F_{X2}(x_2))$ is the product-moment correlation. The rank correlation ($\rho_r(X_1, X_2)$) obtained during the conversion of RVs to uniform RVs lies between $[-1 \quad 1]$. Univariate marginal distribution of a RV is obtained using historical data. While the multivariate marginal distribution of correlated RVs is mostly unknown. Therefore, in such cases, "Copula" theory can be used [200]. In the "Copula" theory, the multivariate distribution is established using the rank information of the correlated one-dimensional cdf [208]. The joint distribution of RVs $X_1 \dots X_m$ (coupled using $C(.)$) with cdfs $F_{X1} \dots F_{Xm}$ is written as follows [203]:

$$F_{X_1,\dots,X_m}(X_1, \dots, X_m) = C\left(F_{X_1}(x_1), \dots, F_{X_m}(x_m)\right) \tag{5.2}$$

Let $F_{Xi}(x_i) = u_i \quad : i = 1, 2, \dots, m$, and u_i is the realisation of uniform variables $U_1 \dots U_m$, then [203]:

$$C(x_1, \dots, x_m) = F_{X_1,\dots,X_m}(F_{X1}^{-1}(u_1), \dots, F_{Xm}^{-1}(u_m)) \tag{5.3}$$

where F_{Xi}^{-1} is the inverse cdf. The process for modelling correlated input RVs using Copula is as follows:

- *Historical data processing:* Hourly data of WPG generation, electrical load demand, and power price in the day-ahead market are collected from the ENTSO-E Transparency Platform [209] and PVGIS platform for the summer (June-August 2020) season of Sardinia, Italy [180]. Normalisation of the data is conducted with respect to the hourly peak value. A univariate distribution is fitted to the data using MATLAB distribution fitter application ($fitdist$). For the obtained WPG generation data, "Weibull distribution" is the best fit pdf. Similarly, the "Normal distribution" best fits the load demand and day-ahead power price data.

- *Computation of Kendell's τ coefficient:* For each pair of correlated input RVs (few exhibit negative correlations), the Kendell's τ coefficients are computed using MATLAB's *corr* function. This exercise is repeated for data pertaining to each hour in the optimisation/scheduling horizon.

- *Correlation modelling:* The Frank copula is used from the Archimedean family (Frank, Gumbel-Hougaard, Clayton) as it can model both negative and positive correlations and handle various dependence structures. Frank copula parameter ϕ_t is

obtained using the τ coefficient obtained in the previous step with the *copulaparam* function of MATLAB. Frank copula is fitted using the observed dependence pattern, followed by generation of correlated RVs. Taking u_{1t} and u_{2t} as inputs, Frank copula function ($C_{Fr}(u_{1t}, u_{2t}|\phi_t)$) returns a joint probability representing the dependence between the corresponding RVs by (5.4) [202]. In (5.4), ln is the natural logarithm,$u_{1t} = F_{X1}(x_{1t})$, and $u_{2t} = F_{X2}(x_{2t})$.

$$\begin{cases} C_{Fr}(u_{1t}, u_{2t}|\phi_t) = \frac{-1}{\phi_t} ln\,(1+g) \\ \text{Where} \quad g = \left(\frac{(e^{-\phi_t u_{1t}}-1)(e^{-\phi_t u_{2t}}-1)}{(e^{-\phi_t}-1)}\right) \end{cases} \tag{5.4}$$

- *Mapping to marginal distributions:* 20,000 data couples are randomly generated for correlated data pairs for each hour using the *copularnd* function of MATLAB. Generated data is mapped back by taking the inverse of the univariate best-fit distribution.

The pdfs used to model the input RVs are summarised in table 5.2. A Monte Carlo dynamic averaging method is used to find the most likelihood value of the input RVs by generating $20,000$ data randomly from the correlated/uncorrelated pdfs for each input RV at each time step. The most likelihood values of input RVs are fed to the EMS of the DCμG.

5.3 EMPC based EMS for normal scheduling

The detailed formulation of the normal scheduling strategy of the DCμG within an EMPC framework is discussed in this section. The objective of the EMS is to maximise the operating profit of the DCμGO considering optimal participation in the aFRR market.

5.3.1 Objective function

During the normal operating period, the objective is to maximise the profit for DCμGO. The problem is formulated in EMPC framework with scheduling horizon $\mathcal{H}_p$ at time k. The objective is as follows: $max(\hat{\Phi})$,i.e., $min(\Phi)$, $\Phi = -\hat{\Phi}$

$$\hat{\Phi} = \sum_{t=0}^{\mathcal{H}_p-1} \sum_{b\in\mathcal{B}} (\pi^{hr} hr^b_{t|k} - \pi^{w} PW^b_{t|k} - \pi^{wc} PWC^b_{t|k} - \pi^{mt} PT^b_{t|k} - \pi^{fc} \delta^{fc,b}_{t|k} - \pi^{bes}(PBC^b_{t|k} + PBD^b_{t|k})) + \pi^{H_2}(m^{H_2,d}_{t|k} - m^{H_2,sh}_{t|k}) - \pi^{ely} - \pi^{g}_{t|k} P^{grid}_{t|k} + \pi^{ur}_{t|k} r^u_{t|k} + \pi^{dr}_{t|k} r^d_{t|k} + \pi^{ed}(PL^b_{t|k} - \sum_{x\in\Xi} pls^{x,b}_{t|k}) \quad : k \in \mathcal{T} \tag{5.5}$$

$t|k$ represents the predicted value at time t based on time k. The first term represents the income from selling the heat recovered from AE. The second and third terms are the cost of procuring power from WPG and its curtailment cost, respectively. The fourth term is the cost of procuring power from MT. The fifth term is the operating cost of FC. The sixth term is the operating cost for BESS. The seventh term denotes the income from H_2 sale. The ninth term is the cost of procuring power from the upstream grid. The tenth and eleventh terms represent the revenue generated by the reservation of capacity for the aFRR up (r^u) and down (r^d) provisions, respectively.

5.3.2 Constraints

The EMS is constrained by the energy balance and physical operating limits of various DER and the DCμG network. The constraints are as follows:

5.3.2.1 Nodal power balance

eq. (5.6) represents the nodal power balance ($\forall k \in \mathcal{T}, \forall b \in \mathcal{B}$) considering the network model of the DCμG [156]. PI is the injected power. $G_{b,n}$ is the b^{th} row and n^{th} column element of bus conductance matrix (G-bus) matrix. Base power is P_{base} (kW). eq. (5.7) denotes that the grid power is considered for bus #1 only where the GIC is connected. eq. (5.8) denotes that electrical load cannot be shedded during normal operation. δ^x is the binary variable for load shedding.

$$\begin{aligned} P^{inj,b}_{t|k} =& \Lambda^b P^{grid}_{t|k} + PW^b_{t|k} + PT^b_{t|k} + PF^b_{t|k} + PBD^b_{t|k} - PBC^b_{t|k} - Pel^b_{t|k} - (PL^b_{t|k} - \sum_{x\in\Xi} pls^{x,b}_{t|k}) \\ &= P_{base} \sum_{n\in\mathcal{B}} G_{b,n} V^n_{t|k} V^b_{t|k} \end{aligned} \tag{5.6}$$

$$\Lambda^b = \begin{cases} 1.0 : b = 1 \\ 0.0; b \in \mathcal{B} \setminus 1 \end{cases} \tag{5.7}$$

$$0 \leq pls_{t|k}^{x,b} \leq \delta_{t|k}^{x,b} \overline{pls}^{x,b}; \quad \delta_{t|k}^{x,b} \in \{0,1\}; \quad \delta_{t|k}^{x,b} = 0; \quad \forall k \in \mathcal{T}_n \cap \mathcal{T}; \forall x \in \Xi \tag{5.8}$$

5.3.2.2 DCμG network operating constraints

eq. (5.9) and eq. (5.10) denote the bus voltage and DCμG feeder current constraints, respectively.

$$0.95 \leq V_{t|k}^b \leq 1.05 : \quad \forall k \in \mathcal{T}, \forall b \in \mathcal{B} \tag{5.9}$$

$$-\overline{\mathcal{I}}^f \leq \mathcal{I}_{t|k}^f \leq \overline{\mathcal{I}^f} : \quad \forall k \in \mathcal{T}, \forall f \in \mathcal{F} \tag{5.10}$$

5.3.2.3 GIC and DG rating constraints

For the related constraints ($\forall k \in \mathcal{T}, \forall b \in \mathcal{B}$) eq. (5.11) denotes the limit on power exchange with the upstream grid. eq. (5.12) denotes that the power generated by the WPG cannot exceed the power generation in the MPPT mode. PW^{avl} is the available wind power as a per unit of the installed capacity $\overline{PW}$ (kW) when the WPG operates in MPPT mode. Deloading the WPG, i.e., deviation from the MPPT point, results in power curtailment given in eq. (5.13). The limits on MT and FC generation are given by eq. (5.14) and eq. (5.15), respectively.

$$\underline{P^{grid}} \leq P_{t|k}^{grid} \leq \overline{P^{grid}} \tag{5.11}$$

$$0 \leq PW_{t|k}^b \leq PW_t^{avl} \overline{PW} \tag{5.12}$$

$$PWC_{t|k}^b = PW_{t|k}^{avl} \overline{PW} - PW_{t|k}^b \tag{5.13}$$

$$\delta_{t|k}^{mt,b} \underline{PT} \leq PT_{t|k}^b \leq \delta_{t|k}^{mt,b} \overline{PT}; \quad \delta_{t|k}^{mt,b} \in \{0,1\} \tag{5.14}$$

$$\delta_{t|k}^{fc,b}\underline{PF} \leq PF_{t|k}^{b} \leq \delta_{t|k}^{fc,b}\overline{PF}; \quad \delta_{t|k}^{fc,b} \in \{0,1\} \tag{5.15}$$

5.3.2.4 BESS constraints

eq. (5.16) gives the energy content status of the BESS. The DOC and DOD constraints are shown in eq. (5.17). The charging and discharging power constraints are given by eq. (5.18). eq. (5.19) denotes that the BESS cannot be simultaneously charged and discharged. The equations for BESS constraints are as follows ($\forall k \in \mathcal{T}, \forall b \in \mathcal{B}$):

$$EB_{t|k}^{b} = EB_{t-1|k}^{b} + \frac{PBC_{t|k}^{b}}{\eta_{bc}} - PBD_{t|k}^{b}\eta_{bd} \tag{5.16}$$

$$0.2\overline{EB}^{b} \leq EB_{t|k}^{b} \leq 0.8\overline{EB}^{b} \tag{5.17}$$

$$\begin{cases} 0 \leq PBC_{t|k}^{b} \leq \delta_{t|k}^{bat,c,b}\overline{PBC}^{b} \\ 0 \leq PBD_{t|k}^{b} \leq (1-\delta_{t|k}^{bat,c,b})\overline{PBD}^{b} \end{cases} \tag{5.18}$$

$$\delta_{t|k}^{bat,c,b} \in \{0,1\} \tag{5.19}$$

5.3.2.5 AE and HSS constraints

The temperature update equation of an AE stack is given by eq. (5.20). The temperature of the AE stack is constrained by eq. (5.21). The volume of the H_2 stored in the HSS is governed by eq. (5.22). The storage level constraints of the HSS are shown in eq. (5.23). eq. (5.24) denotes the limits of the AE power consumption. eq. (5.25) denotes that during normal operation H_2 shedding is zero. The equations for the constraints are as follows ($\forall k \in \mathcal{T}, \forall b \in \mathcal{B}$):

$$\theta_{t|k}^{el,b} = \theta_{t-1|k}^{el,b} + \frac{\frac{(1-\eta_{el})Pel_{t|k}^{b}}{N^{st}} - \frac{(\theta_{t|k}^{el,b}-\theta_{t}^{am})}{R_{heat}^{el}} - hr_{t|k}^{b}}{C_{lmp}^{el}} \tag{5.20}$$

$$60°C \leq \theta_{t|k}^{el,b} \leq 80°C; \quad \theta_{0}^{el,b} = 70°C \tag{5.21}$$

$$VH^b_{t|k} = VH^b_{t-1|k} + \frac{\eta_{el}\left(\frac{Pel^b_{t|k}}{Q^{H_2}_{hhv}}\right) - \frac{PF^b_{t|k}}{Q^{H_2}_{hhv}} - (m^{H_2,d}_{t|k} - m^{H_2,sh}_{t|k})}{\varrho_{H_2}} \tag{5.22}$$

$$\underline{VH} \leq VH^b_{t|k} \leq \overline{VH} \tag{5.23}$$

$$\underline{Pel} \leq Pel^b_{t|k} \leq (1 - \delta^{fc,b}_{t|k})(\overline{Pel} - \underline{Pel}) + \underline{Pel} \tag{5.24}$$

$$m^{H_2,sh}_{t|k} = 0; \quad \forall k \in \mathcal{T}_n \cap \mathcal{T} \tag{5.25}$$

5.3.3 Linearisation of non-convex DCμG network model

Due to the non-affine equality constraint eq. (5.6), the network model becomes non-convex [156]. The convexification of non-affine equality constraints is done using linearisation. The upstream grid is connected to DCμG at bus #1 using a GIC. Also, the bus voltage of bus #1 (i.e., the bus to which the GIC is connected) is maintained at 1.0 p.u.. Therefore, bus #1 is considered as a slack node [182]. Under normal operation, voltages ($V^b_{t,k}$) are close to 1.0 p.u.. We can write the following:

$$V^b_{t,k} = 1 + \Delta V^b_{t,k}; V^n_{t,k} = 1 + \Delta V^n_{t,k}; \quad \Delta v^b_{t,k}, \Delta V^n_{t,k} << 1 \tag{5.26}$$

Therefore, eq. (5.6) can be rewritten as:

$$\begin{aligned}\frac{P^{inj,b}_{t|k}}{P_{base}} &= \sum_{n\in\mathcal{B}} G_{b,n} V^n_{t|k} V^b_{t|k} = \sum_{n\in\mathcal{B}} G_{b,n}(1 + \Delta V^n_{t|k})(1 + \Delta V^b_{t|k}) \\ &= \sum_{n\in\mathcal{B}} G_{b,n}(1 + \Delta V^n_{t|k} + \Delta V^b_{t|k} + \Delta V^n_{t|k}\Delta V^b_{t|k}) \approx \sum_{n\in\mathcal{B}} G_{b,n}(1 + \Delta V^n_{t|k} + \Delta V^b_{t|k})\end{aligned} \tag{5.27}$$

The product $\Delta V^b_{t|k}\Delta V^n_{t|k}$ can be neglected in eq. (5.27), since $\Delta V^n_{t|k}$ and $\Delta V^b_{t|k}$ are small. Using eq. (5.26) in eq. (5.27), we obtain:

$$\frac{P^{inj,b}_{t|k}}{P_{base}} \approx \sum_{n\in\mathcal{B}} G_{b,n}(V^n_{t|k} + V^b_{t|k} - 1) = \sum_{n\in\mathcal{B}} G_{b,n} V^n_{t|k} \tag{5.28}$$

Using the symmetry property of G-bus in eq. (5.28), we can write $\sum_{n\in\mathcal{B}} G_{b,n} = 0$ and $\sum_{n\in\mathcal{B}} G_{b,n}V_{t|k}^{b} = 0$. Therefore, the non-convex nodal power balance equality constraint of eq. (5.6) can be replaced by the linear power flow model given by eq. (5.28). In the matrix form, we can write:

$$[\mathbf{PI}_{t|k}] = P_{base}[\mathbf{G}][\mathbf{\Delta V}_{t|k}] \tag{5.29}$$

Slack bus row and column are removed to obtain an invertible matrix $[\mathbf{G}_{mod}]$ (as $[\mathbf{G}]$ is a singular matrix). Also, from the power injection column, the row corresponding to the slack bus is removed to form $\mathbf{PI}_{t|k}^{mod}$.

$$[\mathbf{\Delta V}_{t|k}^{mod}] = \frac{1}{P_{base}}[\mathbf{G}_{mod}]^{-1}[\mathbf{PI}_{t|k}^{mod}] \tag{5.30}$$

The row and column corresponding to the slack bus, which contains all zero values, are added to the matrix $[\mathbf{G}_{mod}]^{-1}$ to form $\mathcal{G}$. We can write as:

$$[\mathbf{\Delta V}_{t}] = \frac{1}{P_{base}}[\mathcal{G}][\mathbf{PI}_{t|k}] \tag{5.31}$$

Voltage deviation (from 1.0 p.u.) at bus #b is given as:

$$\Delta V_{t|k}^{b} = \frac{1}{P_{base}}\sum_{n\in\mathcal{B}} \mathcal{G}_{b,n}P_{t|k}^{inj,b} \tag{5.32}$$

To measure the impact of power injection change at bus #j on the line current $\mathcal{I}^{f}$ in line #f, GSDF is defined. Therefore, GSDF for line $\#f$ connected between buses $\#b$ and $\#n$ is as follows:

$$GSF^{f,j} = \Delta\mathcal{I}_{t|k}^{f}/\Delta P_{t|k}^{inj,j} \tag{5.33}$$

Where $GSF^{f,j}$ denotes GSDF (p.u) of the DCμG. The line current in $\#f$ is given by:

$$\mathcal{I}_{t|k}^{f} = (\Delta V_{t|k}^{b} - \Delta V_{t|k}^{n})G_{b,n}; \quad g_{b,n} = -G_{b,n} \tag{5.34}$$

Substituting $\Delta V_{t|k}^{b} - \Delta V_{t|k}^{n}$ from eq. (5.32) in eq. (5.34), we get:

$$\mathcal{I}_{t|k}^{f} = (\sum_{j\in\mathcal{B}}(\mathcal{G}_{b,j} - \mathcal{G}_{n,j})P_{t|k}^{inj,j})\frac{g_{b,n}}{P_{base}} \tag{5.35}$$

Therefore, the GSDF from bus $\#k$ to line $\#f$ can be defined as:

$$GSF^{f,j} = \frac{g_{b,n}(\mathcal{G}_{b,k} - \mathcal{G}_{n,k})}{P_{base}} = \frac{-G_{b,n}(\mathcal{G}_{b,k} - \mathcal{G}_{n,k})}{P_{base}} \tag{5.36}$$

Therefore, the network constraint, given by eq. (5.10) can be rewritten in linear form as follows:

$$-\overline{\mathcal{I}}^{f}_{t|k} \leq (\sum_{j \in \mathcal{B}} (\mathcal{G}_{b,j} - \mathcal{G}_{n,j}) P^{inj,j}_{t|k}) \frac{g_{b,n}}{P_{base}} \leq \overline{\mathcal{I}}^{f}_{t|k}; \quad \forall t, k \in \mathcal{T} \tag{5.37}$$

(5.6) and (5.10) are replaced by (5.28) and (5.37), respectively in the EMS model.

5.3.4 Additional constraints for participation in the aFRR market

The DCμGO leverages the flexible DER (MT, BESS, FC, and AE) to participate in the aFRR market by offering up and down reserve provisions.

5.3.4.1 Additional constraints on FC, MT, AE, and HSS for participation in the aFRR market

The MT and FC can provide upward reserve by increasing their power generation. Similarly, the down reserve can be provided by decreasing the power generation of the MT and the FC. The AE can provide an upward reserve by decreasing the power consumption. On the other hand, the AE can provide a downward reserve by increasing the power consumption. eq. (5.38) and eq. (5.39) denote that the upper and lower power limits of the MT should not be exceeded when the upward and downward reserves are activated. eq. (5.40) and (5.41) respectively denote that the upper and lower power limits of the FC cannot be exceeded while providing upward and downward reserves. Similarly, eq. (5.42) and eq. (5.43), respectively, denote that the decrease and increase of AE power consumption for provisioning upward and downward reserves should not violate the lower and upper power consumption constraints of the AE. The constraints are as follows ($\forall k \in \mathcal{T}, \forall b \in \mathcal{B}$):

$$PT^{b}_{t|k} + PT^{b,u}_{t|k} \leq \delta^{mt,b}_{t|k} \overline{PT}; \quad PT^{b,u}_{t|k} \geq 0; \quad \delta^{mt,b}_{t|k} \in \{0,1\} \tag{5.38}$$

$$PT^{b}_{t|k} - PT^{b,d}_{t|k} \geq \delta^{mt,b}_{t|k} \underline{PT}; \quad PT^{b,d}_{t|k} \geq 0; \quad \delta^{mt,b}_{t|k} \in \{0,1\} \tag{5.39}$$

$$PF^{b}_{t|k} + PF^{b,u}_{t|k} \leq \delta^{mt,b}_{t|k}\overline{PF}; \quad PF^{b,u}_{t|k} \geq 0; \quad \delta^{fc,b}_{t|k} \in \{0,1\} \tag{5.40}$$

$$PF^{b}_{t|k} - PF^{b,d}_{t|k} \geq \delta^{fc,b}_{t|k}\underline{PF}; \quad PF^{b,d}_{t|k} \geq 0; \quad \delta^{fc,b}_{t|k} \in \{0,1\} \tag{5.41}$$

$$Pel^{b}_{t|k} - Pel^{b,d}_{t|k} \geq \underline{Pel}; \quad Pel^{b,d}_{t|k} \geq 0 \tag{5.42}$$

$$Pel^{b}_{t|k} + Pel^{b,u}_{t|k} \leq (1 - \delta^{fc,b}_{t|k})(\overline{Pel} - \underline{Pel}) + \underline{Pel}; \quad Pel^{b,u}_{t|k} \geq 0; \quad \delta^{fc,b}_{t|k} \in \{0,1\} \tag{5.43}$$

Furthermore, eq. (5.44) and eq. (5.45) denote that the HSS lower and upper volume constraints should not be violated when the regulation reserves are activated ($\forall k \in \mathcal{T}, \forall b \in \mathcal{B}$). The HSS volume constraint with the activation of the upward regulation reserve is shown in eq. (5.44), while eq. (5.45) illustrates the HSS volume constraint when the downward reserve is activated.

$$\underline{VH} \leq VH^{b}_{t-1|k} + \frac{\eta_{el}\left(\frac{Pel^{b}_{t|k} - Pel^{b,d}_{t|k}}{Q^{H_2}_{hhv}}\right) - \frac{(PF^{b}_{t|k} + PF^{b,u}_{t|k})}{Q^{H_2}_{hhv}} - (m^{H_2,d}_{t|k} - m^{H_2,sh}_{t|k})}{\rho_{H_2}} \leq \overline{VH} \tag{5.44}$$

$$\underline{VH} \leq VH^{b}_{t-1|k} + \frac{\eta_{el}\left(\frac{Pel^{b}_{t|k} + Pel^{b,u}_{t|k}}{Q^{H_2}_{hhv}}\right) - \frac{(PF^{b}_{t|k} - PF^{b,d}_{t|k})}{Q^{H_2}_{hhv}} - (m^{H_2,d}_{t|k} - m^{H_2,sh}_{t|k})}{\rho_{H_2}} \leq \overline{VH} \tag{5.45}$$

5.3.4.2 Additional constraints on the BESS for participation in the aFRR market

The BESS can provide an upward reserve by lowering the charging power if it is already in charging mode. Let $PBC^{b}_{t|k}$ be the charging power just before the upward reserve is to be activated. The reduction in charging power cannot exceed the initial charging power $PBC^{b}_{t|k}$ (eq. (5.46)), and the resulting charging power after the reduction in the charging rate should be lower than the charging power rating of the BESS (eq. (5.47)). If the BESS is already discharging, it can discharge more power to provide the upward reserve without exceeding the power rating of the BESS (eq. (5.48)). Alternatively, if the BESS is already charging, the upward reserve can be provided by stopping the charging process and starting the discharging process (eq. (5.48)). The binary variable $\delta^{b,i}_{t|k}$ is used to depict the

operation mathematically. If $\delta^{b,i}_{t|k} = 1$, the BESS continues in charging mode. Otherwise, it switches over to discharging mode. $PBD^{b}_{t|k}$ denotes the initial discharging power. The BESS can provide the downward reserve by reducing the discharging power by an amount of $PBD^{b,d}_{t|k}$ if it is already operating in the discharging mode with an initial discharging power of $PBD^{b}_{t|k}$ (eq. (5.49)). After reducing discharging power, the new operating point should not violate the BESS power rating (eq. (5.47)). Moreover, the downward reserve can be provided by the BESS by increasing the charging power if it is already in charging mode (eq. (5.51)). Also, if the BESS is in discharging mode, it can stop discharging and start charging to provide the downward reserve (eq. (5.51)). This operation is again controlled by the binary variable $\delta^{b,d}_{t|k}$. eq. (5.52) and eq. (5.53) denote that the DOC and DOD limits of the BESS cannot be violated when the upward and downward reserves are activated, respectively. The constraints are as follows ($\forall k \in \mathcal{T}, \forall b \in \mathcal{B}$):

$$0 \leq PBC^{b,d}_{t|k} \leq PBC^{b}_{t|k} \tag{5.46}$$

$$PBC^{b}_{t|k} - PBC^{b,d}_{t|k} \leq \delta^{b,i}_{t|k}\overline{PBC} : \quad \delta^{b,i}_{t|k} \in \{0,1\} \tag{5.47}$$

$$0 \leq PBD^{b,u}_{t|k} \leq (1-\delta^{b,i}_{t|k})\overline{PBD} - PBD^{b}_{t|k} : \quad \delta^{b,i}_{t|k} \in \{0,1\} \tag{5.48}$$

$$0 \leq PBD^{b,d}_{t|k} \leq PBD^{b}_{t|k} \tag{5.49}$$

$$PBD^{b}_{t|k} - PBD^{b,d}_{t|k} \leq \delta^{b,d}_{t|k}\overline{PBD} : \quad \delta^{b,d}_{t|k} \in \{0,1\} \tag{5.50}$$

$$0 \leq PBC^{b,i}_{t|k} \leq (1-\delta^{b,d}_{t|k})\overline{PBC} - PBC^{b}_{t|k} : \quad \delta^{b,d}_{t|k} \in \{0,1\} \tag{5.51}$$

$$\underline{EB} \leq EB^{b}_{t-1|k} + \frac{(PBC^{b}_{t|k} - PBC^{b,d}_{t|k})}{\eta_{bc}} - (PBD^{b}_{t|k} + PBD^{b,u}_{t|k})\eta_{bd} \leq \overline{EB} \tag{5.52}$$

$$\underline{EB} \leq EB^{b}_{t-1|k} + \frac{(PBC^{b}_{t|k} + PBC^{b,u}_{t|k})}{\eta_{bc}} - (PBD^{b}_{t|k} - PBD^{b,d}_{t|k})\eta_{bd} \leq \overline{EB} \tag{5.53}$$

5.3.4.3 Additional constraints on DCμG network and GIC for participation in the aFRR market

When the upward reserve is activated, the DCμG reduces the power drawn from or injects more power to the upstream AC network through the GIC. On the other hand, for activation of the downward reserve, the DCμG increases the power drawn from or reduces the power injection to the upstream AC network. Let $P^{grid}_{t|k}$ be the initial value of the GIC power before the reservation reserve is activated. The amount of upward reserve ($r^{u}_{t|k}$) is the difference between $P^{grid}_{t|k}$ and $P^{grid,u}_{t|k}$ (eq. (5.54)). Similarly, the available downward reserve ($r^{d}_{t|k}$) is the difference between $P^{grid,d}_{t|k}$ and $P^{grid}_{t|k}$ (eq. (5.55)). When the upward and downward reserves are activated, the GIC power ratings cannot be violated (eq. (5.56) and eq. (5.57)). The nodal power balance with upward and downward reserves activations are shown in eq. (5.58) and eq. (5.59), respectively. Furthermore, the DCμG feeder current and bus voltage limits should not be violated with the activation of reserves (eq. (5.60), eq. (5.61), eq. (5.62), eq. (5.63)).

$$r^{u}_{t|k} = (P^{grid}_{t|k} - P^{grid,u}_{t|k}); \quad r^{u}_{t|k} \geq 0; \quad : \forall k \in \mathcal{T} \tag{5.54}$$

$$r^{d}_{t|k} = (P^{grid,d}_{t|k} - P^{grid}_{t|k}); \quad r^{d}_{t|k} \geq 0; \quad : \forall k \in \mathcal{T} \tag{5.55}$$

$$\underline{P^{grid}} \leq P^{grid,u}_{t|k} \leq \overline{P^{grid}} \quad : \forall k \in \mathcal{T} \tag{5.56}$$

$$\underline{P^{grid}} \leq P^{grid,d}_{t|k} \leq \overline{P^{grid}} \quad : \forall k \in \mathcal{T} \tag{5.57}$$

$$\begin{aligned} P^{inj,b}_{t|k} =& \Lambda^{b}_{t|k} P^{grid,u}_{t|k} + PW^{b}_{t|k} + PT^{b}_{t|k} + PT^{b,u}_{t|k} + PF^{b}_{t|k} + PF^{b,i}_{t|k} + PBD^{b}_{t|k} + PBD^{b,i}_{t|k} \\ & - (PBC^{b}_{t|k} - PBC^{b,d}_{t|k}) - (Pel^{b}_{t|k} - Pel^{b,d}_{t|k}) - (PL^{b}_{t|k} - \sum_{x \in \Xi} pls^{x,b}_{t|k}) \\ & = P_{base} \sum_{n \in \mathcal{B}} G_{b,n} V^{n,u}_{t|k} \Lambda^{b} = 1.0 \quad \forall b = 1, \Lambda^{b} = 0 \quad \forall b \in \mathcal{B} \setminus 1; \forall k \in \mathcal{T}, \forall b \in \mathcal{B}; \forall x \in \Xi \end{aligned} \tag{5.58}$$

$$
\begin{aligned}
P_{t|k}^{inj,b,d} =& \Lambda_{t|k}^{b} P_{t|k}^{grid,d} + PW_{t|k}^{b} + PT_{t|k}^{b} - PT_{t|k}^{b,d} + PF_{t|k}^{b} - PF_{t|k}^{b,d} + PBD_{t|k}^{b} - PBD_{t|k}^{b,d} \\
& - (PBC_{t|k}^{b} + PBC_{t|k}^{b,u}) - (Pel_{t|k}^{b} + Pel_{t|k}^{b,i}) - (PL_{t|k}^{b} - \sum_{x \in \Xi} pls_{t|k}^{x,b}) \\
& = P_{base} \sum_{n \in \mathcal{B}} G_{b,n} V_{t|k}^{n,d} \Lambda^{b} = 1.0 \quad \forall b = 1, \Lambda^{b} = 0 \quad \forall b \in \mathcal{B} \setminus 1; \forall k \in \mathcal{T}, \forall b \in \mathcal{B}; \forall x \in \Xi
\end{aligned}
\tag{5.59}
$$

$$
\mathcal{I}_{t|k}^{f,u} = \sum_{b \in \mathcal{B}} GSF^{f,b} \left(\frac{P_{t}^{inj,b,u}}{P_{base}} \right); -\overline{\mathcal{I}}^{f} \leq \mathcal{I}_{t|k}^{f,u} \leq \overline{\mathcal{I}^{f}} \quad : \forall k \in \mathcal{T}, \forall b \in \mathcal{B}, \forall f \in \mathcal{F} \tag{5.60}
$$

$$
\mathcal{I}_{t|k}^{f,d} = \sum_{b \in \mathcal{B}} GSF^{f,b} \left(\frac{P_{t}^{inj,b,u}}{P_{base}} \right); -\overline{\mathcal{I}}^{f} \leq \mathcal{I}_{t|k}^{f,d} \leq \overline{\mathcal{I}^{f}} \quad : \forall k \in \mathcal{T}, \forall b \in \mathcal{B}, \forall f \in \mathcal{F} \tag{5.61}
$$

$$
0.95 \leq V_{t|k}^{b,u} \leq 1.05 \quad : \forall k \in \mathcal{T}, \forall b \in \mathcal{B} \tag{5.62}
$$

$$
0.95 \leq V_{t|k}^{b,d} \leq 1.05 \quad : \forall k \in \mathcal{T}, \forall b \in \mathcal{B} \tag{5.63}
$$

5.3.5 Solution using the EMPC framework

A general formulation of the DCμG EMS model, described by the objective function eq. (5.5) and the constraints: eq. (5.28), eq. (5.7)-eq. (5.9), eq. (5.37), eq. (5.11)-eq. (5.25), eq. (5.38)-eq. (5.63), for EMPC implementation with a scheduling horizon of $\mathcal{H}_p$ is given below:

$$\max_{\mathcal{U},\partial} \hat{\Phi} = \max_{\mathcal{U},\partial} \sum_{t\in\Omega} \sum_{b\in\mathcal{B}} \hat{\Phi}(\mathcal{X}^b_{t|k}, u^b_{t|k}, \partial^b_{t|k})$$

subject to :

$$\mathcal{G}(\mathcal{X}^b_{t|k}, u^b_{t|k}, \partial^b_{t|k}) \leq 0$$

$$\mathcal{E}(\mathcal{X}^b_{t|k}, u^b_{t|k}, \partial^b_{t|k}) = 0$$

$$\mathcal{X}^b_{t+1|k} = f(\mathcal{X}^b_{t|k}, u^b_{t|k}, \partial^b_{t|k})$$

with $\quad \mathcal{U} = \{u^b_{0|k}, \ldots, u^b_{\mathcal{H}_p-1|k}\}$

$$u^b_{t|k} = \{P^{grid}_{t|k}, PW^b_{t|k}, PWC^b_{t|k}, PT^b_{t|k}, PFC^b_{t|k}, PBC^b_{t|k}, PBD^b_{t|k}, Pel^b_{t|k}, hr^b_{t|k}, PT^{b,u}_{t|k}, PT^{b,d}_{t|k}, PF^{b,u}_{t|k}, PF^{b,d}_{t|k},$$

$$Pel^{b,u}_{t|k}, Pel^{b,d}_{t|k}, PBD^{b,u}_{t|k}, PBC^{b,u}_{t|k}, PBD^{b,d}_{t|k}, PBC^{b,d}_{t|k}, P^{grid,u}_{t|k}, P^{grid,d}_{t|k}, V^b_{t|k}, \mathcal{I}^l_{t|k}, V^{b,u}_{t|k}, V^{b,d}_{t|k}, \mathcal{I}^{l,u}_{t|k}, \mathcal{I}^{l,d}_{t|k}, r^u_{t|k}, r^d_{t|k},$$

$$pls^{x,b}_{t|k}, m^{H_2,sh}_{t|k}\}$$

$$\partial = \{\partial^b_{0|k}, \ldots, \partial^b_{\mathcal{H}_p-1}\}, \quad \partial^b_{t|k} = \{\delta^{fc,b}_{t|k}, \delta^{bat,c,b}_{t|k}, \delta^{bat,d,b}_{t|k}, \delta^{mt,b}_{t|k}, \delta^{u,b}_{t|k}, \delta^{d,b}_{t|k}, \delta^{x,b}_{t|k}\}; \quad \forall x \in \Xi$$

$$\mathcal{X}^b_{t|k} = \{VH^b_{t|k}, \theta^{el,b}_{t|k}, EB^b_{t|k}\}$$

$$\Omega = [k, k + \mathcal{H}_p - 1], \quad \forall k \in \mathcal{T}$$

(5.64)

The following steps are adopted to solve the EMPC based problem defined in (5.64).

1. RES generation and load profiles are sampled over a prediction horizon $\mathcal{H}_p$ at time k. The initial values of state variables ($\mathcal{X}$) and AE efficiency are given as input values for the EMPC problem.

2. Over the prediction horizon, the problem formulated in (5.64) is modelled as a MILP optimisation problem. The solution of this MILP problem will give the optimal control sequence ($\mathcal{U}$).

3. Using the principle of "receding horizon control" [210], only the first sample of $\mathcal{U}$ (i.e., $u^b_{0|k}$) is chosen as optimal control action, and the remaining are discarded.

4. Based on the optimal control sequence, the states ($\mathcal{X}$) are updated for time $k+1$.

5. The prediction horizon is receded by increasing time k to $k+1$, and steps $1-4$ are repeated till the entire optimisation window $\mathcal{T}$ (24 hour in this work) is covered.

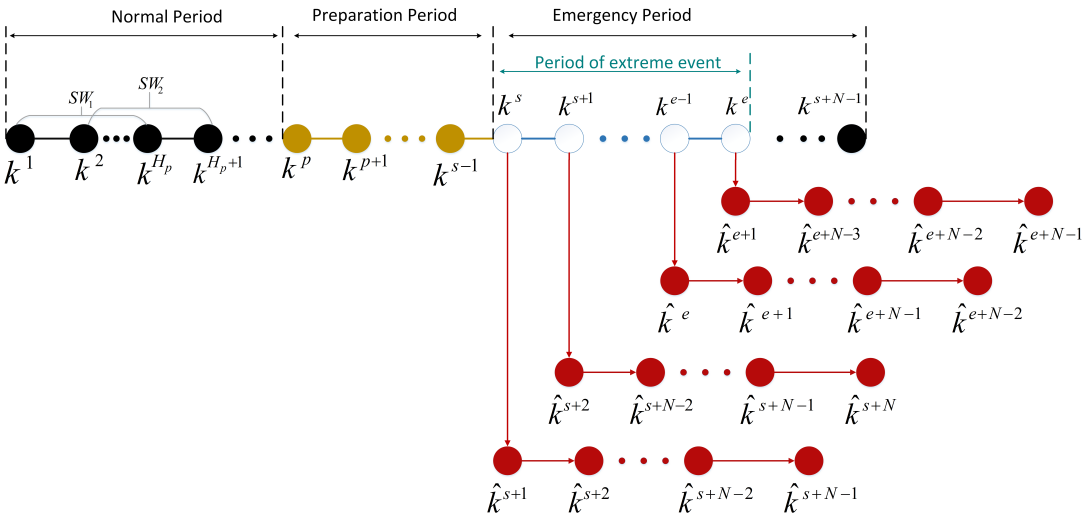

Figure 5.2: Schematic of different periods.

5.4 R-MPCE for resilience-oriented economic scheduling

A resilient scheduling model is also incorporated to enhance the reliability of the proposed EMS. The problem is formulated with the following assumptions:

- The exact time of occurrence of the extreme event is unknown. However, a prediction of the time window within which the extreme event will occur is available with the DCμGO [12]. The extreme event can occur anytime between $[k^s, k^e]$.

- The resilience of the scheduling strategy, i.e., the "resilience index", is assessed using the criticality criterion. According to the criticality criterion, it is essential to maintain supply to the critical loads over the normal scheduling horizon ($N = 24$ hours in this chapter) after the extreme event occurs [74, 207].

- Since the extreme event's exact occurrence time is unknown, the R-MPCE is designed to satisfy the criticality criterion over a time horizon of $k^e - k^s + N$. The above strategy implies that the critical loads are supplied for at least 24 hours even when the extreme event occurs at k^e. For instance, if it is predicted that the extreme event will occur anytime between $[15, 22]$ hours, then the DCμG is prepared to maintain supply to the critical loads for $22 - 15 + 24 = 31$ hours. If the extreme event occurs at $k = 15$, the critical loads can be supplied for 31 hours. On the other

hand, if the extreme event occurs at $k = 22$, the critical loads can be supplied for 24 hours. The proposed philosophy ensures that the criticality criterion is always met.

- Without any loss of generality, the extreme event is a hurricane [12]. During the hurricane, the WPG and the upstream grid are disconnected to avoid potential device damage and propagation of adverse impact. The AE also ceases to function to provide additional reserves during the emergency.

A multi-stage operational framework is considered for the R-MPCE. A schematic is shown in fig. 5.2. Specifically, three stages, described below, are considered based on the timing of the events.

- **Stage 1- Economic operation (k^1 to k^{p-1}):** This is the normal scheduling stage, as the extreme event is not approaching. The objective of DCμGO is to maximise the profit while participating in the energy and the aFRR market. The scheduling window (SW) with the prediction horizon $\mathcal{H}_p$ slides forward with a time granularity of 1 hour. The problem is formulated as per (5.64).

- **Stage 2- Proactive preparation (k^p to k^{s-1})**: In this stage, a proactive preparation is done to prepare the DCμG for the upcoming emergency event. As the SW slides from k^p to k^s, the future emergency event which may occur at k^s or later is sensed. From a preparation point of view, the worst-case scenario is the event occurring at k^s since the preparation time will be the least. Considering the minimum time for the preparation makes the EMS robust by finishing the optimal preparation before the event can occur. Therefore, the proactive preparation is finished at k^{s-1}. The prediction horizon for this stage adaptively changes to $\mathcal{H}_p + k^e - k^s + N - 1$ to satisfy the criticality criterion. N is 24 hours.

- **Stage 3- Emergency operation (k^s to k^{e+N}):** The extreme event can occur anytime between k^s and k^e. Let the extreme event's occurrence time be k^{s+c}.

  - **Stage 3a:** For the period $[k^s, k^{s+c-1}]$ (i.e., the period between the end of proactive preparation and the instant at which the extreme event strikes), the load demand is met using power from the main grid using electricity from

the wholesale market, the WPG, and the MT. The AE remains connected to generate H_2 to meet the H_2 demand. However, the HSS and BESS are not discharged during this period to maintain the energy reserve for meeting the criticality criterion after the extreme event occurs. The objective is to maximise the operating profit of the DCμGO with minimum curtailment of electricity demands. The DCμGO cannot participate in the aFRR market since the emergency can occur anytime, leading to disconnection from the upstream grid.

– **Stage-3b:** The main grid is disconnected at k^{s+c} when the extreme event strikes. Further, the WPG and the AE are turned off. The objective for the period $[k^{s+c}, k^{e+N}]$ is to maintain supply to critical electrical loads, minimise the shedding of moderate and flexible electrical loads, and minimise curtailment of H_2 demand. The chosen period, i.e., $[k^{s+c}, k^{e+N}]$, meets the criticality criterion even under the worst-case scenario.

The data preparation strategy incorporating uncertainty modelling is illustrated in fig. 5.3, while the overall scheduling framework is depicted in fig. 5.4. In fig. 5.3, data is processed with careful consideration of the correlations among the RVs, ensuring that the resulting dataset is suitable for integration into the proposed architecture. fig. 5.4 outlines the three key operational stages: economic operation, proactive preparation, and emergency operation. The data prepared in fig. 5.3 is consistently utilised across all these stages. During normal operating conditions, the system engages the economic operation phase, relying on the data obtained from fig. 5.3. As a potential emergency is detected, the strategy transitions sequentially into the proactive preparation and then the emergency operation phase, both continuing to utilise the same dataset prepared through fig. 5.3.

5.4.1 Problem formulation under normal operation

During normal operation, the EMS formulated in the EMPC framework, described in eq. (5.64), is adopted. However, the optimisation period is $\mathcal{T}_n$ (i.e., k^1 to k^{p-1}) instead of $\mathcal{T}$.

5.4.2 Problem formulation for proactive preparation

The aim of the EMS is to minimise the operating cost (or maximise the profit) during the proactive operation duration and simultaneously prepare the DCμG for the upcoming emergency event. The preparation entails satisfaction of the criticality criteria and minimum flexible and moderate load curtailment during the upcoming emergency operating period. The objective related to the preparation requirement is translated into financial terms in the overall objective. Therefore, extra terms related to the cost of shedding flexible, moderate, and critical electrical loads, and H_2 demand curtailment are added to the objective function defined in eq. (5.64). The priority of supplying critical loads is the highest, while the priority of supplying flexible loads is the lowest. The priority of moderate load lies in between. Subsequently, the penalty cost for shedding critical load has the highest value, and that of flexible has the lowest. The penalty cost of shedding a moderate load lies in between. The objective function for proactive preparation is as follows:

$$\hat{\Phi}_p = \max_{\mathcal{U},\partial} \sum_{t\in\widetilde{\Omega}} \sum_{b\in\mathcal{B}} \hat{\Phi}(\mathcal{X}^b_{t|k}, u^b_{t|k}, \partial^b_{t|k}) - \min_{\widetilde{\mathcal{U}},\widetilde{\partial}} \sum_{t\in\widetilde{\Omega}} \sum_{b\in\mathcal{B}} \sum_{x\in\Xi} (\gamma^{x,b}_{t|k} pls^{x,b}_{t|k}) + \gamma^{H_2}_{t|k} m^{H_2,sh}_{t|k}$$

with

$$\begin{aligned}
&\widetilde{\mathcal{U}} = \{\widetilde{u}^b_{0|k}, \ldots, \widetilde{u}^b_{\mathcal{H}_{p-1}|k}\}; \quad \Xi \in [flex, mod, crit] \\
&\widetilde{u}^b_{t|k} = \{pls^{flex,b}_{t|k}, pls^{mod,b}_{t|k}, pls^{crit,b}_{t|k}\} \\
&\widetilde{\partial} = \{\widetilde{\partial}^b_{0|k}, \ldots, \widetilde{\partial}^b_{\mathcal{H}_{p-1}}\} \quad \widetilde{\partial}^b_{t|k} = \{\delta^{flex,b}_{t|k}, \delta^{mod,b}_{t|k}, \delta^{crit,b}_{t|k}\} \\
&\widetilde{\Omega} = [k, k + k^e + N], \quad \forall k \in [k^p, k^{s-1}]
\end{aligned} \tag{5.65}$$

Subject to: eq. (5.28), eq. (5.7), eq. (5.9),eq. (5.37), eq. (5.11)-eq. (5.24), eq. (5.38)-eq. (5.63)

$$\delta^{x,b}_{t|k} = 0 \quad \forall t < k^p; \quad \forall x \in \Xi, \forall b \in \mathcal{B} \tag{5.66}$$

$$0 \leq pls^{x,b}_{t|k} \leq \delta^{x,b}_{t|k} \overline{pls}^{x,b}; \quad \forall x \in \Xi, \forall b \in \mathcal{B} \tag{5.67}$$

$$P^{grid}_{t|k} = Pel^b_{t|k} = PW^b_{t|k} = 0 \quad \forall t \geq k^s, \forall k; \quad \forall b \in \mathcal{B} \tag{5.68}$$

$$PT^{b,u}_{t|k} = PT^{b,d}_{t|k} = PF^{b,u}_{t|k} = PF^{b,d}_{t|k} = Pel^{b,u}_{t|k} = Pel^{b,d}_{t|k} = PBC^{b,i}_{t|k} = PBC^{b,d}_{t|k} = PBD^{b,u}_{t|k} = PBD^{b,d}_{t|k} = r^{u}_{t|k} = r^{d}_{t|k} = P^{grid,u}_{t|k} = P^{grid,d}_{t|k} = 0; \quad \forall t \geq k^s, \forall k, \quad \forall b \in \mathcal{B} \tag{5.69}$$

γ^x is the penalty cost for shedding electrical loads of different priorities. γ^{H_2} is the penalty cost for curtailing H_2 demand. The additional constraints related to (5.65) are given by eq. (5.66)-eq. (5.69). The load-shedding should not occur before proactive preparation (eq. (5.66)). The limit of load shedding is given by eq. (5.67). The DCμG gets islanded, the WPG stops generation, and the AE ceases to operate after the extreme event occurs (eq. (5.68)). eq. (5.69) denotes that the DCμG does not participate in the aFRR market during the emergency.

5.4.3 Problem formulation for emergency period

5.4.3.1 Stage 3a

The objective is to maximise the operational profit of the DCμGO, supply critical electrical loads with minimum curtailment of moderate and flexible electrical loads, and minimise curtailment of H_2 demand. The DCμG remains connected to the upstream grid. The WPG and AE remain on. However, the DCμG does not participate in the aFRR market due to the imminent emergency. The objective function is given in eq. (5.70). The limits of load curtailment are shown in eq. (5.71). The BESS cannot discharge, and the volume of H_2 stored in the HSS should not reduce from the level achieved at the end of the proactive preparation period (eq. (5.72)). eq. (5.72) ensures sufficient energy storage for the criticality criterion. eq. (5.73) denotes that the DCμG does not participate in the aFRR market.

$$\hat{\Phi}_p = \max_{\mathcal{U},\partial} \sum_{t\in\widetilde{\Omega}} \sum_{b\in\mathcal{B}} \hat{\Phi}(\mathcal{X}^b_{t|k}, u^b_{t|k}, \partial^b_{t|k}) - \min_{\widetilde{u},\widetilde{\partial}} \sum_{t\in\widetilde{\Omega}} \sum_{b\in\mathcal{B}} \sum_{x\in\Xi} (\gamma^{x,b}_{t|k} pls^{x,b}_{t|k}) + \gamma^{H_2}_{t|k} m^{H_2,sh}_{t|k}$$

with

$$\begin{aligned}
&\widetilde{\mathcal{U}} = \{\widetilde{u}^b_{0|k}, \ldots, \widetilde{u}^b_{\mathcal{H}_{p-1}|k}\}; \quad \Xi \in [flex, mod, crit] \\
&\widetilde{u}^b_{t|k} = \{pls^{flex,b}_{t|k}, pls^{mod,b}_{t|k}, pls^{crit,b}_{t|k}\} \\
&\widetilde{\partial} = \{\widetilde{\partial}^b_{0|k}, \ldots, \widetilde{\partial}^b_{\mathcal{H}_{p-1}}\} \quad \widetilde{\partial}^b_{t|k} = \{\delta^{flex,b}_{t|k}, \delta^{mod,b}_{t|k}, \delta^{crit,b}_{t|k}\} \\
&\widetilde{\Omega} = [k, k^e + N], \quad \forall k \in [k^s, k^{s+e-1}]
\end{aligned} \tag{5.70}$$

Subject to: eq. (5.28), eq. (5.7), eq. (5.9),eq. (5.37), eq. (5.11)-eq. (5.24)

$$0 \leq pls^{x,b}_{t|k} \leq \delta^{x,b}_{t|k} \overline{pls}^{x,b}; \quad \forall x \in \Xi, \forall b \in \mathcal{B} \tag{5.71}$$

$$PBD^b_{t|k} = 0; \quad vh_{t|k} \geq vh_{k^{s-1}}; \quad \forall t \geq k^s, \forall k, \quad \forall b \in \mathcal{B} \tag{5.72}$$

$$\begin{aligned}
&PT^{b,u}_{t|k} = PT^{b,d}_{t|k} = PF^{b,u}_{t|k} = PF^{b,d}_{t|k} = Pel^{b,i}_{t|k} = Pel^{b,d}_{t|k} = PBC^{b,u}_{t|k} = PBC^{b,d}_{t|k} = PBD^{b,u}_{t|k} = \\
&PBD^{b,d}_{t|k} = r^u_{t|k} = r^d_{t|k} = P^{grid,u}_{t|k} = P^{grid,d}_{t|k} = 0; \quad \forall t \geq k^s, \forall k, \quad \forall b \in \mathcal{B}
\end{aligned} \tag{5.73}$$

5.4.3.2 Stage 3b

In the emergency period, the sole objective is to minimise load shedding while ensuring the supply to critical loads. All the constraints (5.9),(5.37), (5.14)-(5.19), (5.22)-(5.24) should be satisfied. The horizon for emergency period is taken as 24 hour to meet the critical criterion. Also, the rolling horizon structure of EMPC is not used and the problem is formulated as a basic MILP optimisation problem. The problem is formulated as follows:

$$\begin{aligned}
&\hat{\Phi}_e = \min_{\mathcal{U}\cup\widetilde{\mathcal{U}},\partial\cup\widetilde{\partial}} \sum_{t\in\Omega_c} \sum_{b\in\mathcal{B}} \sum_{x\in\mathcal{L}} (\gamma^{x,b}_t pls^{x,b}_t) + \gamma^{H_2}_t m^{H_2,sh}_t \\
&\text{S.t.} \quad (5.9), (5.37), (5.14) - (5.19), (5.22) - (5.24) \\
&\text{with} \quad \Omega_c \in [k^s, k^{s+N-1}]
\end{aligned} \tag{5.74}$$

$$PT_t^b + PF_t^b + PBD_t^b - PBC_t^b - PL_t^b + pls_t^{x,b} = P_{base} \sum_{n \in \mathcal{B}} G_{b,n} V_t^n; \quad \forall t \in \Omega_c, \forall x \in \mathcal{L} \quad (5.75)$$

Where (5.75) is the additional constraint for nodal power balance equation during emergency period where grid, AE, and WPG are disconnected from the DCμG.

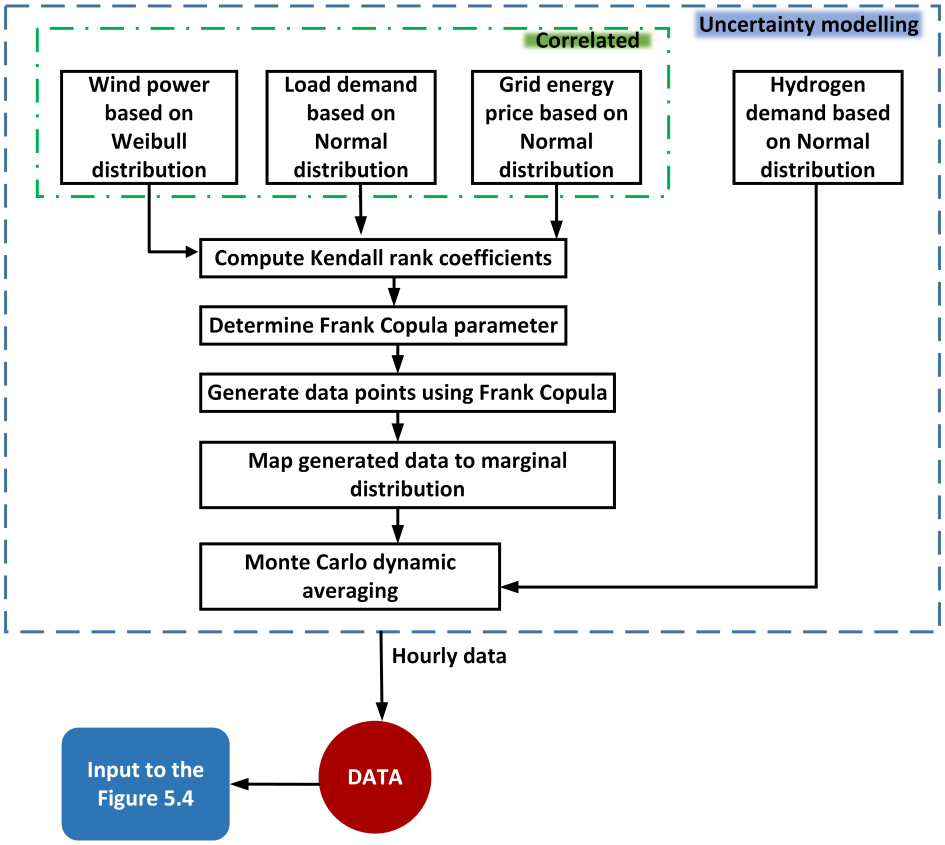

Figure 5.3: Probabilistic data preparation

5.5 Simulation and Results

5.5.1 Test System

A modified version of the six (#6) bus, seven (#7) line DCμG test system is considered for simulation studies [61]. The base power and voltage are 230 kW and 380 V, respectively. The test system comprises a WPG, FC, AE, MT, BESS, and HSS unit. Detailed information, including data and the location of each unit, is provided in table 5.4. fig. 5.5

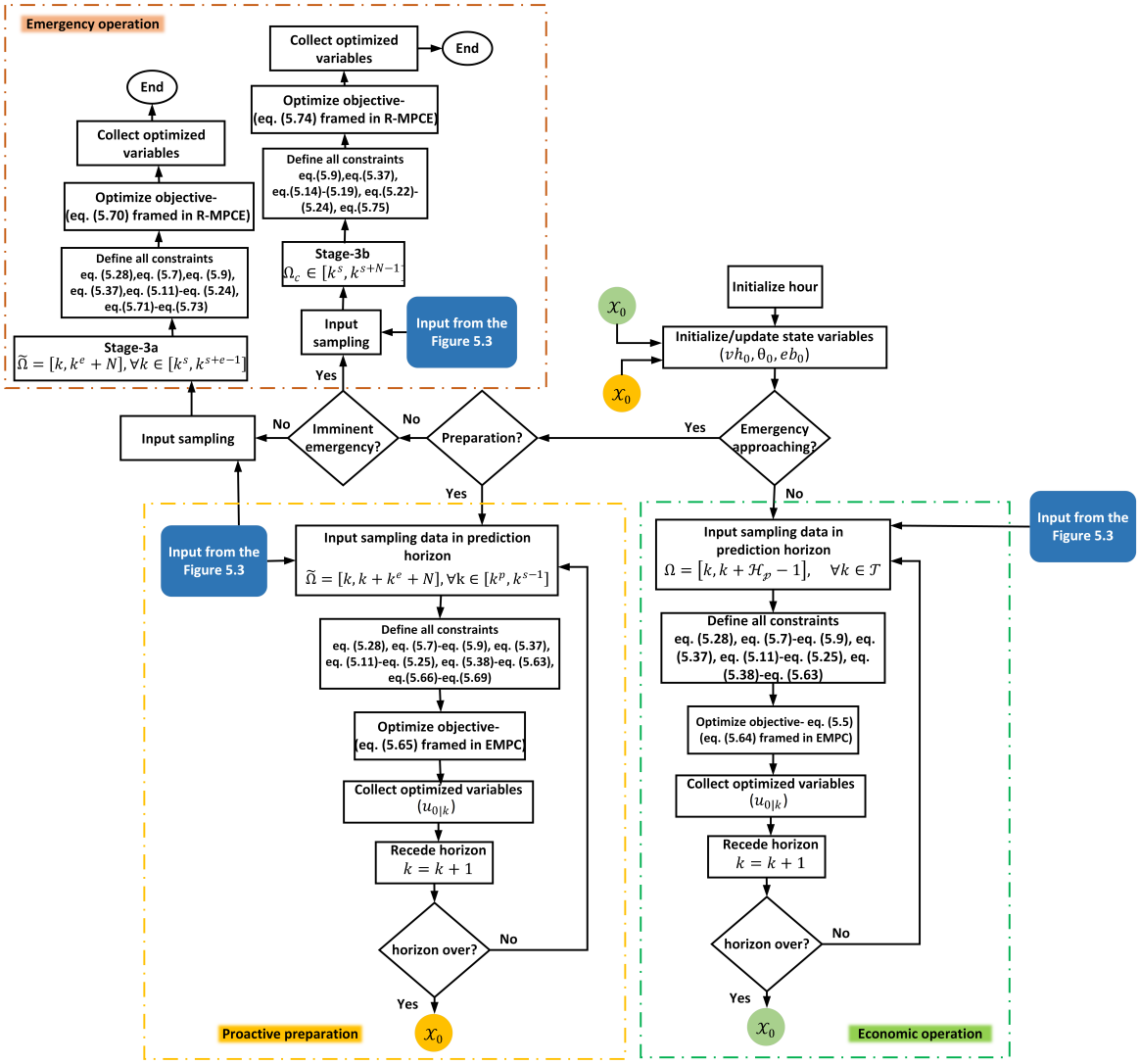

Figure 5.4: Flowchart of the proposed approach

gives the hourly profile of electricity demand, H_2 demand, WPG generation, and wholesale electricity price. Load on each bus of DCμG is classified as flexible (60% of bus load), moderate (20% of bus load), and critical (20% of bus load) load. The penalty costs of shedding flexible, moderate, and critical loads are 0.52 ($/kW), 1.04 ($/kW), and 1.56 ($/kW), respectively. Also, the cost of shedding H_2 demand load is 8 ($/kg). The model was developed in MATLAB R2019a with a YALMIP toolbox and GUROBI solver on a desktop with Intel(R) Core(TM) i7-12700 CPU @2.10GHz and 16 GB RAM.

5.5.2 Simulation cases

Several simulation cases are analysed in this study. The simulation cases are detailed in table 5.3. Further, it is predicted that the extreme event can occur anytime between

hours #15 and #21, i.e., between $k = 15$ and $k = 21$. Also, the proactive preparation time is three hours. In other words, the proactive preparation period lasts from hour #12 to hour #14, i.e., for $k = 12$ to $k = 14$. In the worst-case scenario, the extreme event occurs at $k = 15$, i.e., at hour #15. We have considered the worst-case scenario in the simulation. To establish the critical criterion, the system should be prepared to supply the critical load for the next normal schedule horizon (24 hours). Therefore, the total scheduling horizon is taken as 38 hours in this work.

Table 5.3: Simulation cases

Simulation cases	Participation in the aFRR market	R-MPCE
Case-1(C#1)	✗	✗
Case-2(C#2)	✓	✗
Case-3(C#3)	✗	✓
Case-4(C#4)	✓	✓

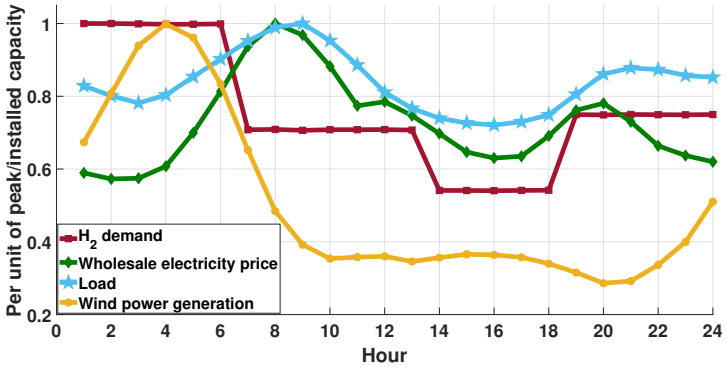

Figure 5.5: Hourly generation, demand, and price profile

Table 5.4: Test System Data

GIC	Location- Bus#1, $\overline{P^{grid}} = 100$ kW
WPG	Location- Bus#3, $\overline{PW} = 30$ kW, $\pi^{w} = 0.0342$\$/kW
FC	Location-Bus#3, $\overline{PF} = 50$ kW, $\pi^{fc} = 0.133$\$kW
MT	Location-Bus#3, $\overline{PT} = 20$kW, π^{mt} =0.1614 \$/kW
BESS	Location- Bus#2, $\overline{EB} = 30$kWh, $EB_0 = 9$kWh, $\overline{PBC} = 15$kW, $\overline{PBD} = 15$kW, $\pi^{bes} = 0.006$\$kW
AE	Location-Bus#3, $\overline{Pel} = 150$kW, $\underline{Pel} = 6.5$kW, $\overline{VH} = 1.6Nm^3$, $\underline{VH} = 0.4Nm^3$, $VH_0 = 0.9Nm^3$, $\pi^{ely} = 0.107$\$, $\pi_{H2} = 5$\$/kg, $\eta_{el} = 0.68$, $R^{el}_{heat} = 18C/kW$, $C^{el}_{lmp} = 0.0833kW/C$,$Q^{H_2}_{hhv} = 39.4$kWh/kg, ϱ_{H_2}=7.8 kg/Nm^3
Bus load (peak value)	Bus#2-25 kW, Bus#4- 25 kW, Bus#5- 50 kW, $\pi^{ed} = 0.18$ \$/kW.

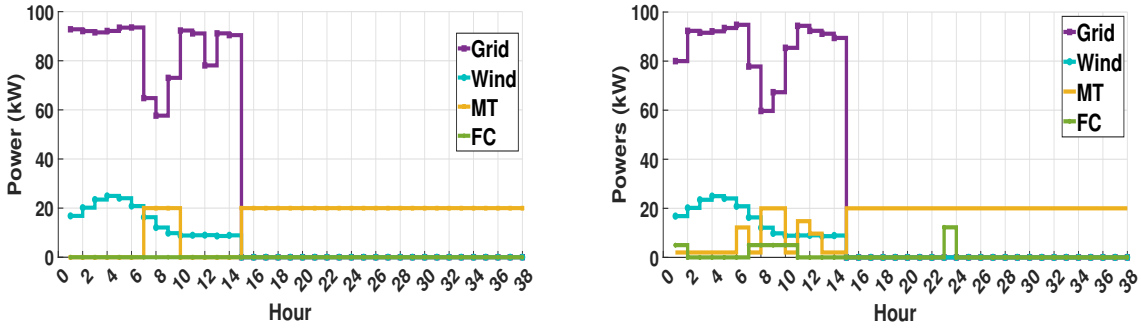

(a) C#1

(b) C#2

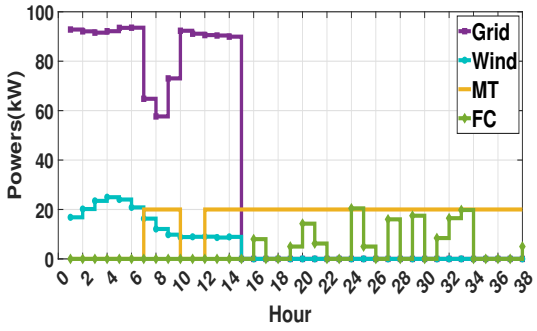

(c) C#3

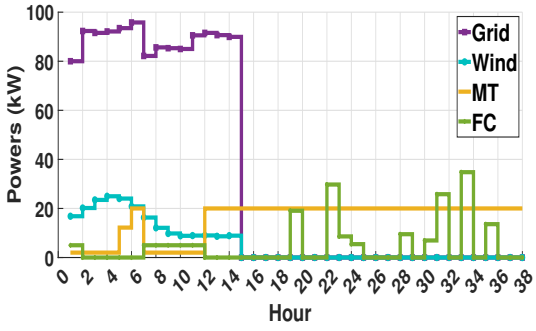

(d) C#4

Figure 5.6: Hourly generation

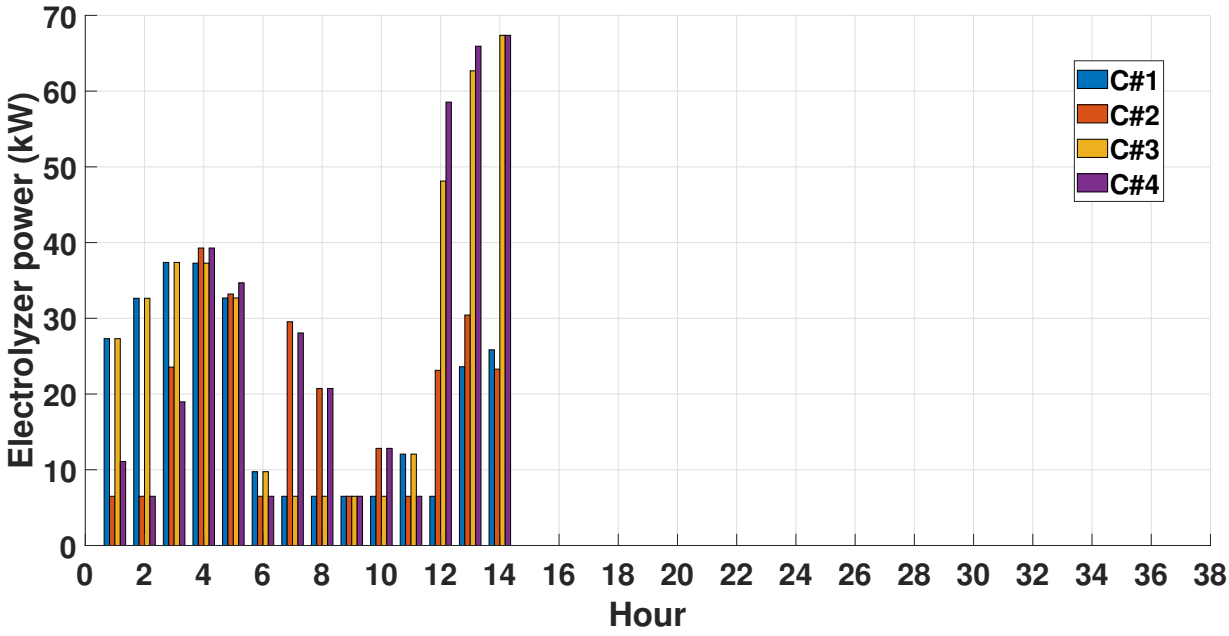

Figure 5.7: Hourly power consumed by AE

5.5.3 Results

5.5.3.1 Case-1(C#1)

In this case, the DCμGO does not participate in the aFRR market. Also, resilient scheduling is not considered, i.e., proactive preparation before the emergency is not incorporated.

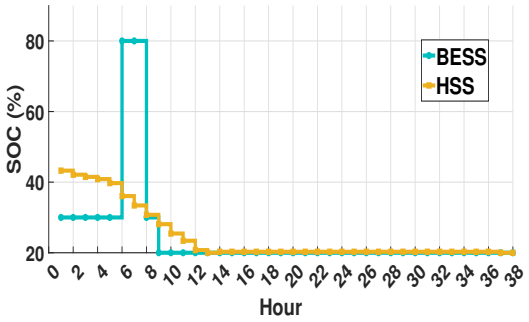

(a) C#1

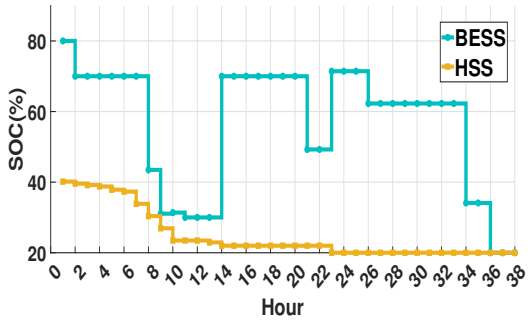

(b) C#2

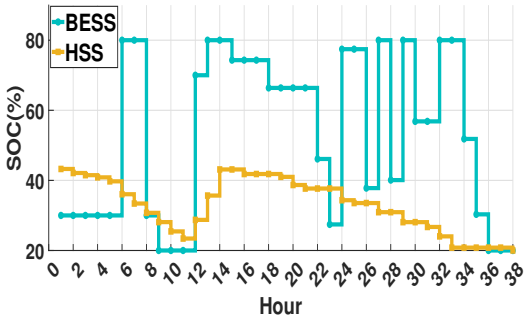

(c) C#3

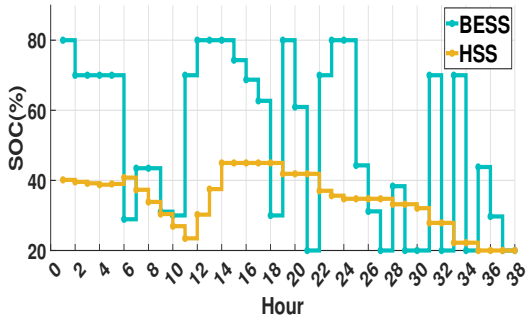

(d) C#4

Figure 5.8: Hourly Storage

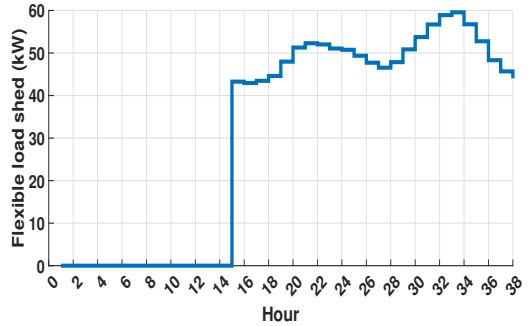

(a) Flexible load shedding

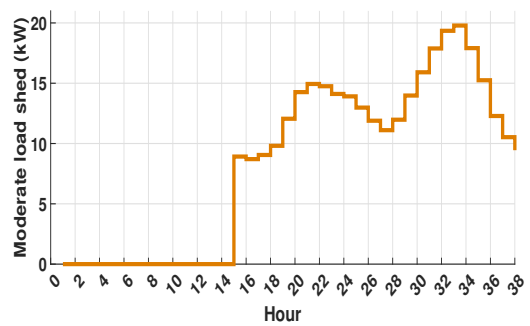

(b) Moderate load shedding

Figure 5.9: Hourly load shedding for C#1

The hourly electricity procurement and generation profiles before and after the extreme event are shown in fig. 5.6a. The electricity price in the wholesale market is low during hours $\#1 - \#6$ (see fig. 5.5). Therefore, electricity is procured from the wholesale market/upstream grid (see fig. 5.6a). Further, the AE uses the electricity procured from the wholesale electricity market/upstream grid (see fig. 5.7) to generate H_2 for meeting the high H_2 demand during hours $\#1 - \#6$ (see fig. 5.5). When the wholesale market

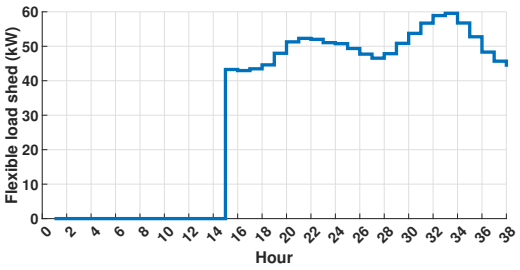

(a) Flexible load shedding

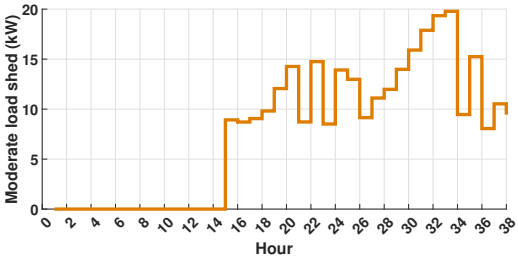

(b) Moderate load shedding

Figure 5.10: Hourly load shedding for C#2

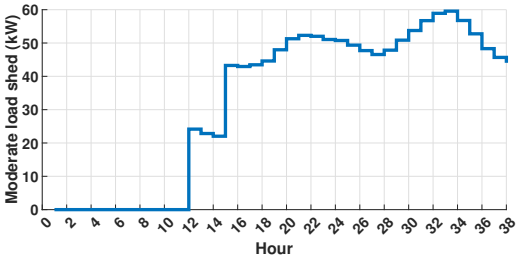

(a) Flexible load shedding

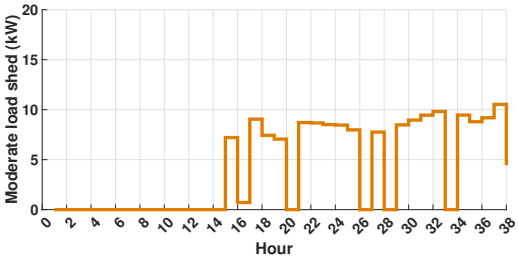

(b) Moderate load shedding

Figure 5.11: Hourly load shedding for C#3

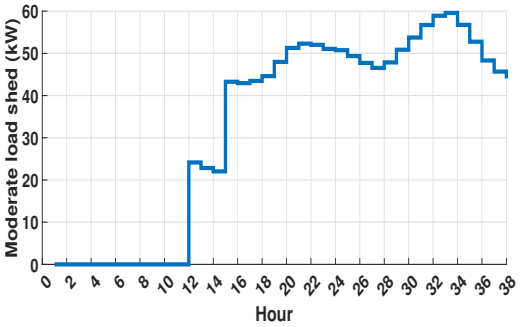

(a) Flexible load shedding

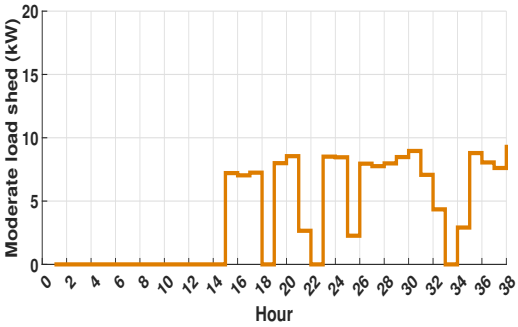

(b) Moderate load shedding

Figure 5.12: Hourly load shedding for C#4

electricity price is higher, i.e., during hours #7 – #10, producing electricity using the MT is economical. The BESS charges to the maximum capacity using the electricity generated by the MT during hours #6 – #8 (see fig. 5.8a). The DCμG switches to island mode of operation, and the WPG and AE are turned off during the emergency operating period (hour #15 onwards) (see fig. 5.6a and fig. 5.7). All the flexible loads are shed (see fig. 5.9a), and some of the moderate loads are also shed (see fig. 5.9b) to utilise the available energy for meeting the critical load requirement. From fig. 5.8a, it is seen that

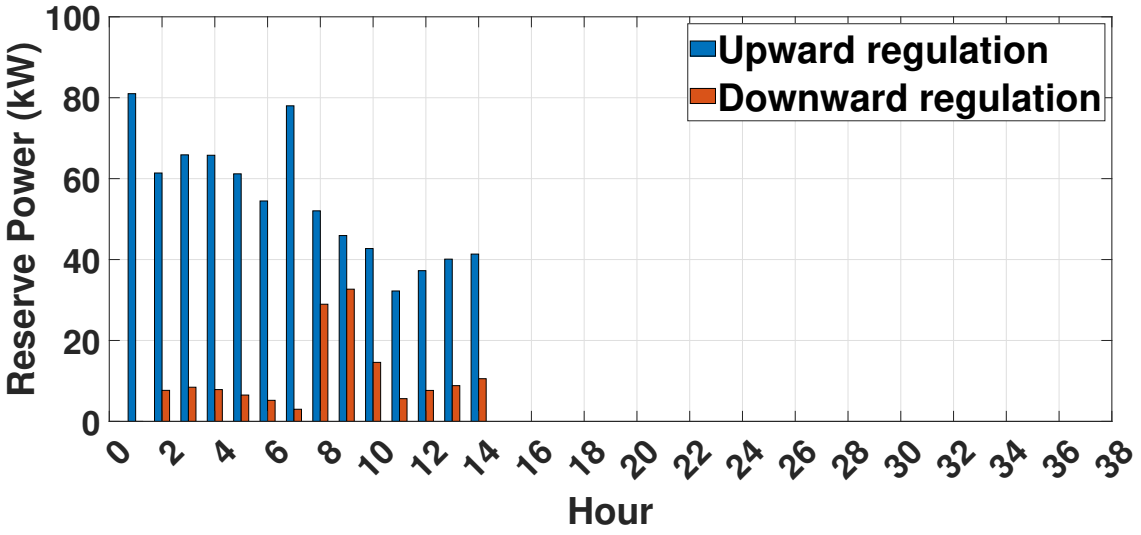

(a) C#2

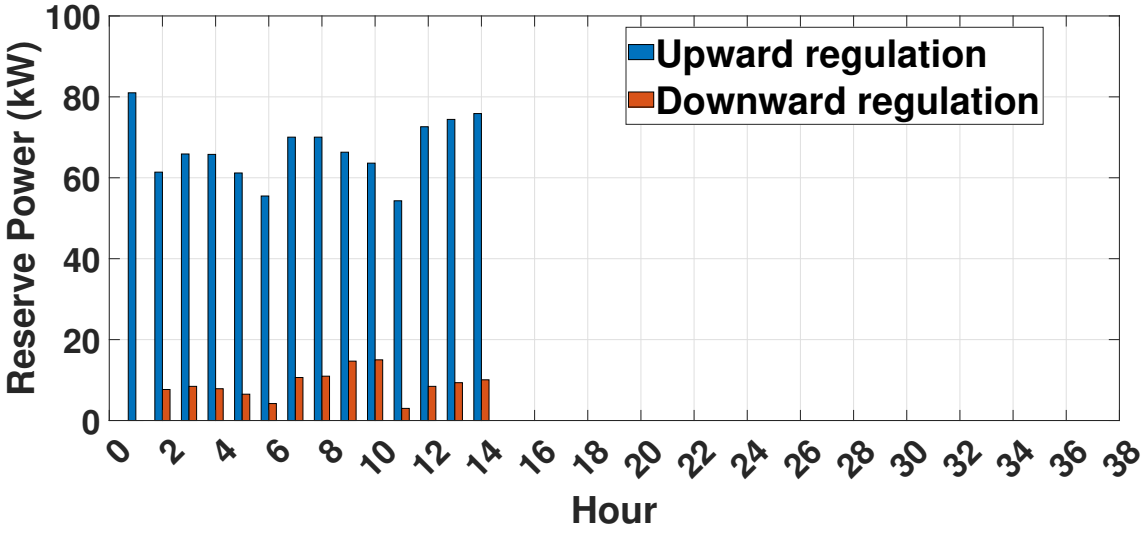

(b) C#4

Figure 5.13: Up/Down reserves under normal period

due to economic reasons, BESS and HSS reach the DOD limits before the extreme event. Therefore, the BESS and HSS-FC combination fail to meet the moderate and critical load demands during the emergency period, and a large proportion of the moderate loads are also shed (see fig. 5.9b). The FC remains off throughout the scheduling horizon.

The total cost of procuring and generating electricity is 172.57 $ during the normal operating period (i.e., from hour $\#1 - \#14$). The total income from sales of H_2, heat, and electricity is 262.50 $. Therefore, the total profit during the normal operating period

is 89.93 $. During the emergency period, the total cost of electrical and H_2 demand curtailment is 1064.33 $.

5.5.3.2 Case-2(C#2)

In this case, the DCμGO participates in the aFRR market. However, the resilience aspect is not incorporated in the scheduling algorithm. In other words, the scheduling strategy does not include proactive preparation before the emergency. As in case C#1, the DCμGO meets most of the electricity demand by procuring electricity from the wholesale electricity market during hours $\#1-\#5$ since the electricity price in the wholesale market is low during this period. However, since the DCμG participates in the aFRR market, the MT is on and generates minimum power (2 kW) during hours $\#1-\#5$, so that upward reserves can be provided if needed. thus enabling DCμGO to participate in aFRR market (see fig. 5.6b). However, the MT cannot provide downward reserves during this period since it is operating at the minimum rating. During hours $\#8-\#10$, the MT operates at the maximum capacity, thus offering down reserves only. The MT can offer upward and downward reserves for the remaining hours before the extreme event. Similarly, FC operates at the minimum capacity and can provide upward reserve only during hour #1 and hours $\#7-\#10$. The hourly electricity consumption of the AE during the normal period is shown in fig. 5.7. From the fig. 5.7, we observe that during the first hour, the AE operates at the minimum capacity, thus offering downward reserves only. However, the AE can provide upward and downward reserves during hours $\#2-\#7$, and hours $\#11-\#14$ AE. The SOC of the BESS and HSS are shown in fig. 5.8b. The H_2 demand is met by discharging the H_2 stored in the HSS and H_2 generated by the AE during the normal operating period. Therefore, the level of H_2 stored in the HSS reduces (see fig. 5.8b) and the AE also produces H_2 (see fig. 5.7) during periods of high H_2 demand (hours $\#1-\#6$). The BESS can offer upward reserves by increasing the discharging power or by lowering the charging power. On the other hand, BESS has to increase the charging power or reduce the discharging power to provide downward reserves. Note that the resilience aspect is not incorporated in the scheduling scheme, and economic operation is the sole objective. The BESS and HSS reach DOD limits before the emergency period due to the economic scheduling of the DCμG (see fig. 5.8b). Therefore, the BESS and the HSS-FC combination cannot support the electricity requirement during the emergency

operating period. Since MT is the only electricity generation source during the emergency operating period, all flexible loads (see fig. 5.10a) and most moderate loads (see fig. 5.10b) are shed. Therefore, the DCμG system is not prepared for the upcoming extreme event when the resilience-oriented scheduling is not carried out. The FC remains off for the entire scheduling horizon.

The total cost of procuring and generating electricity is 183.12 $ during the normal operating period (hours $\#1-\#14$). Total income from participation in the aFRR market and the sale of electricity, H_2, and heat is 300.51 $. Therefore, the total profit during the normal operating period is 117.38 $. The total cost of electrical and H_2 demand shedding during the emergency period is 1036.33 $.

5.5.3.3 Case-3(C#3)

R-MPCE is considered in this case. However, the DCμGO does not participate in the aFRR market. A proactive preparation strategy is adopted in which the DCμG prepares for the upcoming extreme event. The electricity procured from the wholesale market/upstream grid and electricity produced by various DERs are shown in fig. 5.6c. The wholesale market electricity price is lower during hours $\#1-\#6$ (see fig. 5.5). Therefore, the bulk of the electricity demand is met by purchasing electricity from the wholesale electricity market/upstream grid (see fig. 5.6a). When the wholesale market electricity price is higher, i.e., during hours $\#7-\#10$, generating electricity using the MT is economical. The HSS and BESS discharge to meet electricity and H_2 demand during the normal operating period (see fig. 5.8c). However, both BESS and HSS charge during the proactive preparation period (i.e., hours $\#12-\#14$) so that the stored energy can be utilised during the emergency period (see fig. 5.8c). Electricity is purchased from the wholesale electricity market/upstream grid and generated by the MT to charge BESS and HSS during the preparation period (see fig. 5.6c). When the emergency period starts, both BESS and HSS are utilised to feed the electricity demands. The FC utilises the stored H_2 in HSS to generate electricity for catering to the electricity demand during the emergency period (refer to fig. 5.6c). Also, MT operates at rated capacity to meet the electricity demand (see fig. 5.6c). Further, shedding of moderate electrical loads during the emergency period is lower than that in cases C#1 and C#2 since BESS and HSS are used to feed the loads (see fig. 5.11b).

The total cost of procuring/generating electricity and H_2 and flexible load shedding during the normal operation and proactive preparation periods (i.e., from hour $\#1-\#14$) are 183.89 \$ and 47.52, respectively. Note that a small amount of electrical and H_2 demands are curtailed (see fig. 5.11a) during proactive preparation to utilise the available electricity to charge the BESS and HSS units. The total income from the sale of H_2, heat, and electricity is 245.75 \$ during normal operation and proactive preparation. Therefore, the total profit during normal operation and proactive preparation is 14.34 \$. During the emergency period, the total cost of shedding flexible and moderate electrical loads and H_2 demand is 898.16 \$.

5.5.3.4 Case-4(C#4)

We have considered R-MPCE operation of the DCμG with participation in the aFRR market in this case. fig. 5.6d shows the hourly electricity procurement from the wholesale market/upstream grid and electricity generated by DERs. The MT is on and generates minimum power (2 kW) during hours $\#1-\#5$ and hours $\#7-\#11$ (see fig. 5.6b). If the upward reserve needs to be activated, the MT can increase its electricity generation. On the other hand, the MT cannot provide downward reserves during this period since it is already operating at the minimum power limit. The MT operates at its maximum capacity during hours $\#6-\#7$ and cannot provide upward reserves during this period. However, the MT can provide downward reserves equal to its capacity (20 kW) during this period of operation. The MT can offer upward and downward reserves for the remaining hours before the extreme event. Similarly, the FC operates at its minimum capacity during hour #1 and hour $\#7-\#12$. Therefore, the FC can provide upward reserves only during this period of operation. The AE operates at the minimum capacity during hour #1 (see fig. 5.7). Therefore, the AE can provide a downward reserve during this period. The AE operates between the minimum and maximum power ratings and can provide upward and downward reserves during hours $\#2-\#6$ and hours $\#12-\#14$.

The BESS and HSS discharge to meet electricity and H_2 demands during the normal operating period, i.e., during hours $\#1-\#11$ (see fig. 5.8d). However, the BESS and HSS start charging with the onset of the proactive preparation period (hours $\#12-\#14$) to meet the resiliency criterion of DCμG operation (see fig. 5.8d). Apart from meeting the electricity demand of the customers, electricity is also used to charge the BESS and

produce H_2 using the AE to charge the HSS. Therefore, the electricity demand increases during proactive preparation and is met by procuring electricity from the wholesale market and generating electricity using the MT (see fig. 5.6d).

The MT operates at rated capacity to meet the electricity demand during the emergency period (see fig. 5.6d). Also, the FC consumes H_2 from the HSS to generate electricity for meeting the electricity demand during the emergency period, i.e., from hour #15 onwards (see fig. 5.6d). The BESS also discharges during the emergency period to meet the electricity demand. Further, shedding of moderate load is lower than that in cases C#1 and C#2 since the BESS and HSS are used to feed the loads (see fig. 5.12b). The total cost of procuring and generating electricity from different sources is 194.03 $ during normal operation and proactive preparation (hours $\#1 - \#14$). As in case C#3, a small amount of electrical and H_2 demands are curtailed (see fig. 5.12a) during proactive preparation to fully utilise the available electricity for charging the BESS and HSS for meeting the resiliency criterion during the emergency period. The cost of electrical and H_2 demand curtailment during proactive preparation is 47.52 $. The total revenue of the DCμGO from participation in aFRR market and sale of H_2, heat, and electricity is 290.07 $ during normal operation and proactive preparation. Therefore, the total profit during normal operation and proactive preparation is 48.52 $. The total cost of shedding electrical (flexible and moderate loads) and H_2 demand is 886.31 $ during the emergency period. Compared to C#1, the cost of curtailment during the emergency period in C#4 is $\sim$ 16.72% lower.

5.5.4 Impact of Resilient operation, participation in the aFRR market, and duration of proactive preparation

5.5.4.1 Impact of Resilient operation

The objective is to investigate the impact of incorporating resiliency requirements in the scheduling strategy on the operating economy and load curtailment. For the same, we compare cases C#1 and C#3 (see table 5.5). The operating cost in C#3 is $\sim$ 6.56% higher than in C#1 since the BESS and HSS charge during proactive preparation in C#3. By contrast, in C#1, the BESS and HSS discharge during the said hours from economic considerations. Further income from the sale of electricity and H_2 also reduces slightly in

C#3 since a small amount of flexible load is curtailed during the proactive preparation to utilise the available electricity for charging the BESS and the HSS for resilient operation after islanding. The AE consumes more electricity in C#3 during proactive preparation (see fig. 5.7) to increase the volume of H_2 in the HSS for resilient operation. Therefore, the income from heat sale is $\sim 70.16\%$ higher in case C#3 than in case C#1 (see table 5.5). The DCμGO profit during the normal and preparation period for case C#3 is 75.6$ lower than case C#1. However, the R-MPCE in case C#3 reduces the curtailment cost during the emergency period by 166.17 $ compared to case C#1. Therefore, the higher operating cost and lower profit for R-MPCE (case C#3) is overshadowed by the reduction in the curtailment cost, making R-MPCE economically viable and attractive considering the complete scheduling horizon.

5.5.4.2 Impact of participation in the aFRR market

The aim is to investigate and quantify the economic impact of DCμGO's participation in the aFRR market. We compare cases C#1 and C#2 for the purpose. The operating cost is $\sim 10.56\%$ higher (C#2) when the DCμG operates in the aFRR market. The operating cost is higher in C#2 because the FC and the MT turn on and operate at minimum power ratings for a particular duration within the scheduling horizon for providing upward reserves support. Note that the FC and MT are off in C#1 since buying power from the wholesale electricity market during these periods is economical. However, the additional income from participation in the aFRR market overshadows the higher operating cost, and the DCμGO profit is $\sim 30.51\%$ higher with participation in the aFRR market (see table 5.5). Therefore, participation in the aFRR market provides an additional source of revenue for the DCμGO, making the operation financially rewarding.

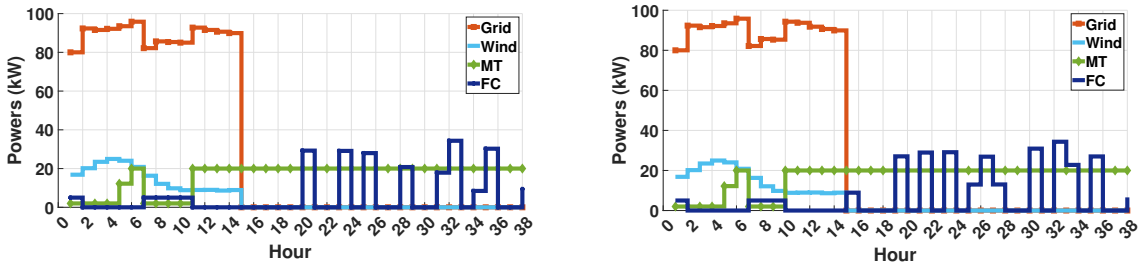

(a) 4 hour preparation time

(b) 5 hour preparation time

Figure 5.14: Hourly generation for different proactive preparation time

Table 5.5: Comparison of Cases

Performance Index		Cases			
		*C#1	*C#2	C#3	C#4
Normal period with proactive preparation	Operational cost ($)	172.57	183.13	183.89	194.03
	Cost of shedding H_2 load ($)	0	0	11.63	11.63
	Cost of shedding flexible load ($)	0	0	35.89	35.89
	Income from heat sale ($)	4.19	5.45	7.13	8.58
	Income from H_2 sale ($)	42.67	42.67	35.4	35.4
	Income from up regulation ($)	0	30.32	0	38.01
	Income from down regulation ($)	0	6.42	0	4.86
	Income from load sell ($)	215.65	215.65	203.22	203.22
Emergency period	Cost of shedding flexible load ($)	623.21	623.21	623.21	623.21
	Cost of shedding moderate load ($)	333.62	305.27	167.10	155.25
	Cost of shedding critical load ($)	0	0	0	0
	Cost of shedding H_2 load ($)	107.51	107.85	107.85	107.85
Profit during normal and proactive preparation period ($)		**89.94**	**117.38**	**14.34**	**48.52**
Curtailment cost during emergency period ($)		**1064.33**	**1036.33**	**898.16**	**886.31**

*Cases without proactive preparation period

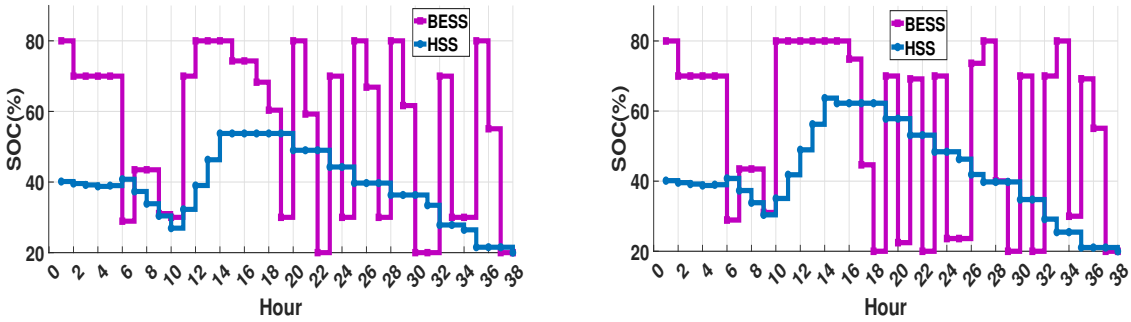

(a) 4 hour preparation time

(b) 5 hour preparation time

Figure 5.15: Hourly Storage for different proactive preparation time

5.5.4.3 Impact of the duration of proactive preparation

We have investigated the impact of the duration of proactive preparation on the operating economy during normal and proactive preparation and on the demand curtailment during the emergency period. We have studied case C#4 by considering proactive preparation duration of 3 hours, 4 hours, and 5 hours. The comparison results are given in table 5.6. The electricity procurement/generation profiles and status of BESS and HSS for different durations of proactive preparation are shown in fig. 5.14 and fig. 5.15, respectively. The electricity consumption pattern of the AE for varying duration of proactive preparation

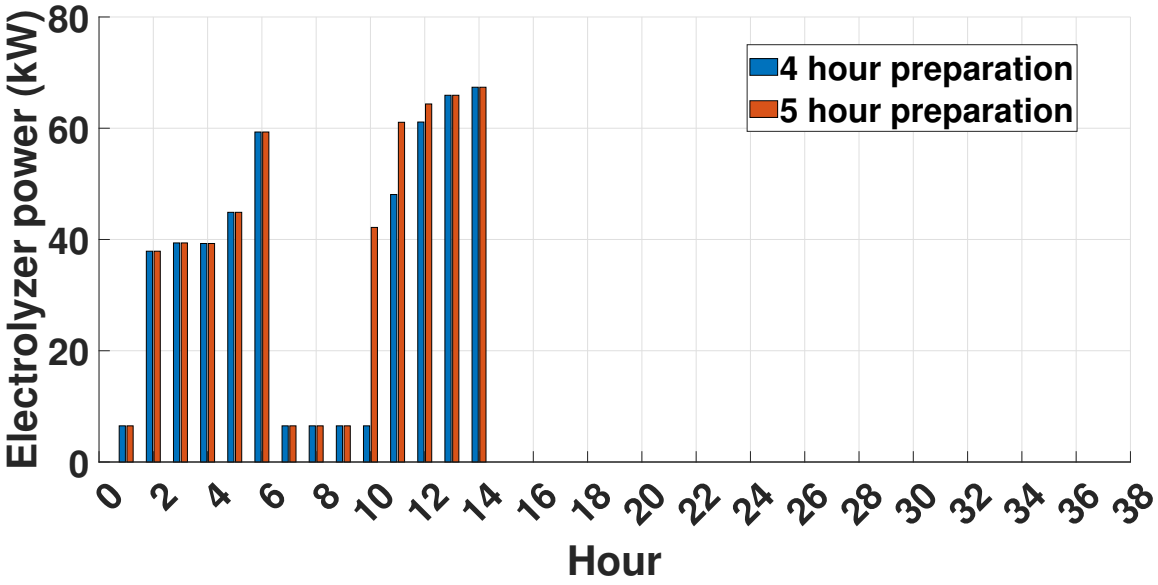

Figure 5.16: Hourly power consumed by AE for different proactive preparation time

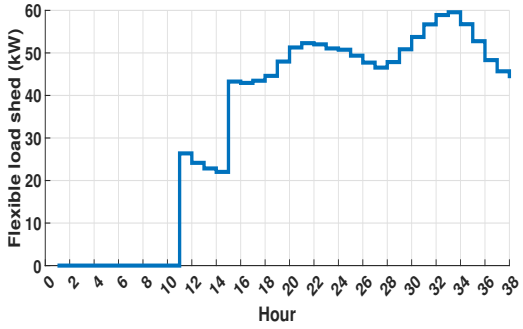

(a) 4 hour preparation time

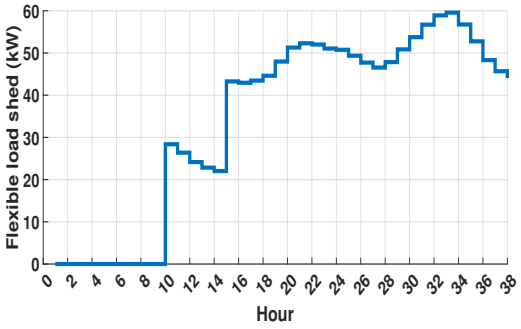

(b) 5 hour preparation time

Figure 5.17: Hourly flexible load shedding for different proactive preparation time

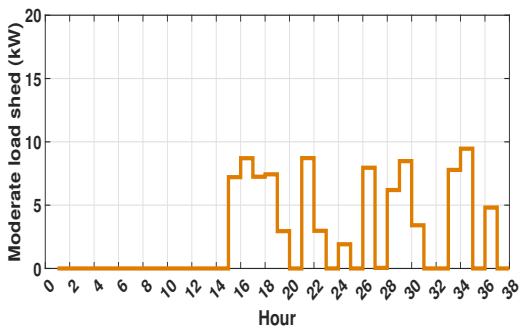

(a) 4 hour preparation time

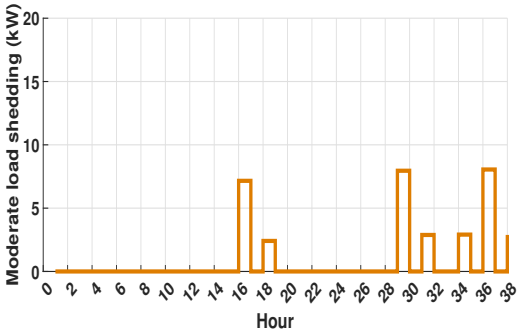

(b) 5 hour preparation time

Figure 5.18: Hourly moderate load shedding for different proactive preparation time

Table 5.6: Results for different preparation times

Performance Index		Preparation time		
		3 hours	**4 hours**	**5 hours**
Normal period with proactive preparation	Operational cost ($)	194.03	196.56	200.38
	Cost of shedding H_2 load ($)	11.63	15.84	20.04
	Cost of shedding flexible load ($)	35.89	49.61	64.36
	Income from heat sale ($)	8.58	9.58	10.83
	Income from H_2 sale ($)	35.4	32.77	30.14
	Income from up regulation ($)	38.01	38.11	38.18
	Income from down regulation ($)	4.86	5.03	4.55
	Income from load sell ($)	203.22	198.47	193.37
Emergency period	Cost of shedding flexible load ($)	623.21	623.21	623.21
	Cost of shedding moderate load ($)	155.25	99.08	35.62
	Cost of shedding critical load ($)	0	0	0
	Cost of shedding H_2 load ($)	107.85	107.85	107.85
Profit during normal and proactive preparation period ($)		**48.52**	**21.95**	**-7.71**
Curtailment cost during emergency period ($)		**886.31**	**830.15**	**766.69**

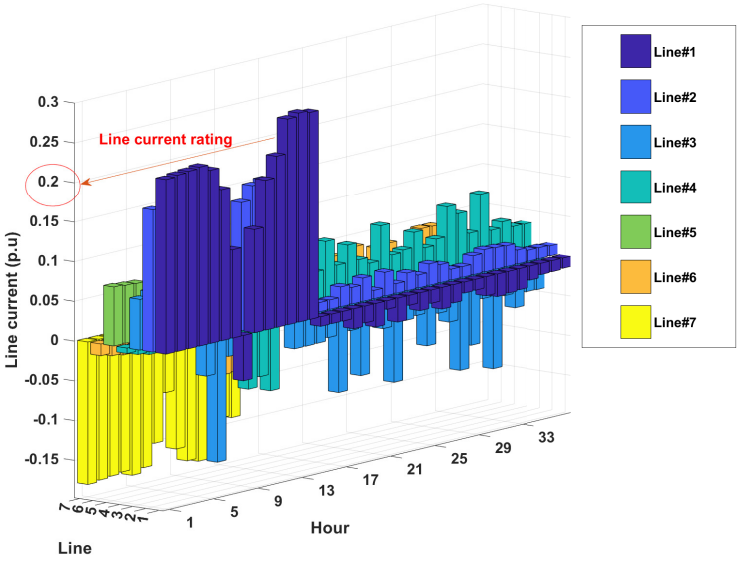

Figure 5.19: Line currents with the method in [12]: Case C#3

is shown in fig. 5.16. Flexible and moderate load curtailments with varying duration of proactive preparation are shown in fig. 5.17 and fig. 5.18, respectively.

The operating cost increases as the duration of proactive preparation increases from 3 to 5 hours. The increased operating cost with higher proactive preparation duration is attributable to the higher energy consumption of AE (consumes electricity for longer duration during the prolonged preparation period to charge the HSS) (see fig. 5.16 and

Table 5.7: Comparison of proposed approach with existing work

Performance Index		C#3	C#4	[12]
Normal period with proactive preparation	Operational cost ($)	183.89	194.03	190.51
	Cost of shedding H_2 load ($)	11.63	11.63	11.63
	Cost of shedding flexible load ($)	35.89	35.89	71.78
	Income from heat sale ($)	7.13	8.58	10.56
	Income from H_2 sale ($)	35.4	35.4	35.4
	Income from up regulation ($)	0	38.01	0
	Income from down regulation ($)	0	4.86	0
	Income from load sell ($)	203.22	203.22	190.80
Emergency period	Cost of shedding flexible load ($/day)	623.21	623.21	623.21
	Cost of shedding moderate load ($)	167.10	155.25	118.02
	Cost of shedding critical load ($)	0	0	0
	Cost of shedding H_2 load ($)	107.85	107.85	107.85
Profit under normal period ($)		**14.34**	**48.52**	**-37.16**
Total Cost under emergency period ($)		**898.16**	**898.16**	**849.09**

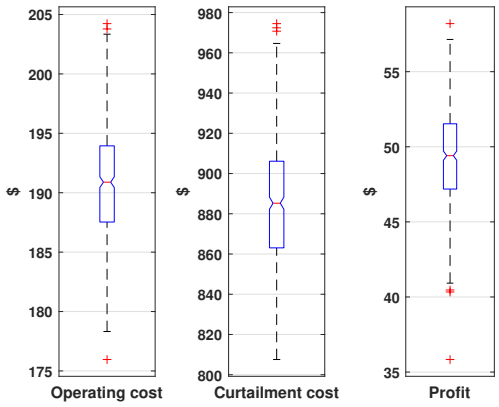

Figure 5.20: Statistical Analysis with variation of input RV

fig. 5.7). The operation of AE during prolonged proactive preparation leads to the volume of H_2 storage in the HSS (compare fig. 5.15b with fig. 5.15a and fig. 5.8d). The higher volume of H_2 available in the HSS at the inception of the emergency period allows the FC to generate electricity (see fig. 5.14b) for a longer duration for meeting the electricity demand within the DCμG. Hence, the moderate electricity demand curtailment is reduced with increasing proactive preparation time (compare fig. 5.18b with fig. 5.18a and fig. 5.12b), resulting in lower curtailment costs. For instance, the curtailment cost is $\sim$ 13.49% lower if the proactive preparation period is 5 hours instead of 3 hours. If the duration of proactive preparation is 4 hours, then the curtailment cost is $\sim$ 7.64%

lower. On the flip side, the operating cost increases significantly, and the profit of the DCμGO during the normal and proactive preparation periods reduces substantially with a higher duration of proactive preparation. Therefore, selecting the duration of proactive preparation is crucial to trade off the economic and resilience considerations of DCμG scheduling strategy and needs an in-depth study in the future.

5.5.5 Comparison with existing work

The performance of the proposed algorithm is compared with the algorithm reported in [12]. aFRR market participation and DCμG network operating security constraints were not considered in [12]. The EMS proposed in [12] leads to the overloading of the line#1 during several hours (see fig. 5.19), thereby underscoring the limitation of implementing the EMS proposed in [12] on practical DCμG networks. By contrast, the EMS proposed in this chapter ensures that line current and bus voltage limits are not violated, which is a strength of this study.

A comparative analysis of the economic performance of the method reported in [12] with cases C#3 and C#4 is shown in table 5.7. The operating cost during the normal period with proactive preparation is $\sim 3.6\%$ higher with the EMS reported in [12] compared to case C#3 (see table 5.7). Also, the profit during the normal period with proactive preparation is much lower with the EMS in [12] (see table 5.7). On the other hand, the curtailment of moderate load during the emergency period is lower with the EMS proposed in [12] (see table 5.7). Moreover, the profit of the DCμGO during the normal operating period increases significantly with participation in the aFRR market (case C#4 proposed in this chapter), underlining the advantage of designing an EMS with aFRR participation capability.

The AE operates at rated power (150 kW) when the EMS reported in [12] is implemented. The DCμG draws maximum electricity from the upstream grid during proactive preparation to store maximum H_2 in the HSS to ensure minimum load curtailment during the impending emergency period when the EMS in [12] is implemented. Consequently, moderate load curtailment is lower during the emergency period, but the operating cost is high during the normal and proactive preparation period. However, high electricity consumption of AE during proactive preparation and high electricity generation by FC during the emergency period lead to line current violation. By contrast, the AE electric-

ity consumption and H_2 stored in the HSS during proactive preparation and electricity generated by the FC during the emergency period is constrained by line current capacity when the EMS proposed in this chapter is implemented. This leads to higher profit (lower operating cost) during the normal and proactive preparation periods but higher curtailment of moderate load.

5.5.6 Discussion on algorithm scalability

The proposed model is formulated as a MILP problem. MILP has been used frequently with success in various power system optimisation problems like combined cooling, heat and power system operation planning [211], long-term energy mix planning [212], optimal scheduling for multi-carrier coupled gas-electricity system [213], optimal planning of RES allocation [214], day-ahead scheduling of power systems [215, 216], ancillary services market participation of SPG-BESS systems [217], energy scheduling and resilience enhancement schemes for integrated energy hubs [12, 78], etc. It has already been observed in [216] that the MILP approach can successfully handle power scheduling problems for power system islands with a limited number of generators.

The binary variables in the present formulation are associated with the ON/OFF status of FC, MT, and the charge/discharge status of BESS. Since the present chapter deals with the operation problem (short-term problem) of a DCμG, it is expected that even if the size of the DCμG increases, there will be a limited number of DER in the system, and hence only a limited number of binary variables will be present in the model. Moreover, since the MPC approach is used in this work, the optimisation in each time step is limited to the prediction horizon, which is less than a day-ahead optimisation problem. Therefore, the dimension of the problem in each optimisation time step is limited in the proposed formulation. Also, the MILP approach is more scalable with a lower computation burden compared to a non-linear programming problem and easily solvable with available commercial solvers like GUROBI and CPLEX [213]. Therefore, the proposed algorithm will be scalable for DCμG EMS applications. Further, commercial solvers like GUROBI offer the flexibility of tuning the parameters for improving the convergence of large-scale MILP problems according to available guidelines [218]. Also, some recent studies have reported methods like "surrogate absolute-value Lagrange Relaxation" to improve the convergence of large-scale MILP problems [219], which can also used to solve the proposed

model if needed.

5.5.7 Statistical analysis with input RV variability

In order to conduct a statistical analysis of the impact of input RV variability, we have conducted a MCS with 500 trials. Each input RV is generated randomly from its pdf considering 10% standard deviation around the mean value for every hour. Note that the standard deviations in this test are higher than those obtained based on the historical data and considered in the earlier Monte Carlo dynamic averaging. Higher variations are considered purposely to assess the impact of worst-case variation of input RVs on the EMS. The EMS is run for each trial, and the statistical analysis is presented as box plots in fig. 5.20. The inter-quartile range (IQR) of the operating cost (during normal and proactive preparation period) is 16.70 \$, which is $\sim 8.77\%$ of the median value of 190.44 \$. Similarly, the IQR of the curtailment cost during the emergency period is 43.07 \$, i.e., $\sim 4.86\%$ of the median value of 885.26\$. The operating profit of the DCμGO has an IQR of 4.34 \$, which is 8.85% of the median value of 49.10\$. Therefore, the proposed EMS has acceptable robustness even with the variation of multiple input RVs.

5.6 Conclusions

This chapter presents an EMS for a DCμG focusing on resilience. The DCμG comprises WPG, BESS, AE, FC, and HSS. The electrical loads are categorised as critical, moderate, and flexible demands. The DCμG operates in the grid-connected mode under normal conditions and participates in the aFRR market to enhance resource utilisation. The DCμG operation is divided into three periods: normal, proactive preparation, and emergency. The DCμG switches over to islanded mode, and the WPG turns off to prevent potential device damage during the emergency, i.e., after the extreme event strikes. The objective of the EMS is to maximise total profit during the normal operating period. The objective during the proactive preparation period is maximising profit and preparing the DCμG for the impending extreme event. On the other hand, during the emergency period, the objective is to supply all critical loads and minimise curtailment of moderate and flexible loads. Therefore, the AE also turns off during the emergency period to utilise the H_2 stored in the HSS for producing electricity using the FC to meet the criticality criterion

of resilient operation. The contribution of this work is to formulate the EMS simultaneously incorporating the economic and resilient aspects of electricity-H_2 DCμG operation considering the participation of the DCμG in the aFRR market in a convex optimisation framework. Additional equipment-level and DCμG network-level operating constraints are formulated to incorporate the effect of DCμG participation in the aFRR market. Further, input uncertainties of RES generation, electricity demand, wholesale electricity price, H_2 demand, and their correlations are modelled in a Frank Copula-embedded MCS framework. The optimisation problem is cast in a MPC framework using the concept of receding horizon. The proposed EMS is validated by simulation studies on a six-bus test electricity-H_2 DCμG system. Following are some key findings:

- Without resilience, the system is unprepared for the impending extreme events, thus causing flexible and moderate load curtailment. Therefore, the curtailment cost is $\sim 15.61\%$ higher than the resilience-oriented approach without aFRR market participation.

- Participation in the aFRR market increases profit during the normal period by $\sim 30.51\%$, offering additional revenue for the DCμGO.

- During the emergency period, the proposed scheme (considering proactive preparation and aFRR market participation) has $\sim 16.72\%$ lower curtailment cost than the case without proactive preparation and aFRR market participation.

- A more extended preparation period improves the system's resilience at the expense of economic benefits during normal mode of operation. Therefore, a reasonable selection of the duration of proactive preparation is essential in achieving a trade-off between the economy during normal operation and load curtailment during the emergency period.